Precambrian Research 282 (2016) 52–73

Contents lists available at ScienceDirect

Precambrian Research

journal homepage: www.elsevier.com/locate/precamres

An 850–820 Ma LIP dismembered during breakup of the Rodinia supercontinent and destroyed by Early Paleozoic continental subduction in the northern Tibetan Plateau, NW China

Xin Xu [a], Shuguang Song [a,*], Mark B. Allen [b], Richard E. Ernst [c,d], Yaoling Niu [b,e], Li Su [f]

[a] MOE Key Laboratory of Orogenic Belt and Crustal Evolution, School of Earth and Space Sciences, Peking University, Beijing 100871, China
[b] Department of Earth Sciences, Durham University, Durham DH1 3LE, UK
[c] Department of Earth Sciences, Carleton University, Ottawa K1S 5B6, Canada
[d] Faculty of Geology and Geography, Tomsk State University, Tomsk, Russia
[e] Institute of Oceanology, Chinese Academy of Science, Qingdao 266071, China
[f] Geological Lab Center, China University of Geosciences, Beijing 100083, China

ARTICLE INFO

Article history:
Received 11 October 2015
Revised 31 May 2016
Accepted 11 July 2016
Available online 22 July 2016

Keywords:
North Qaidam LIP
Dolerite dike and basalt
Eclogite
Mantle plume
Breakup of Rodinia
Continental subduction

ABSTRACT

Neoproterozoic intraplate magmatism is widely distributed in NW China and generally thought to be related to the breakup of the Rodinia supercontinent. Here we report a fragmented Large Igneous Province (LIP) formed at 850–820 Ma in the northern margin of the Qaidam block, northern Tibetan Plateau (named herein as the "North Qaidam LIP"). The associated rocks have undergone various grades of metamorphism from greenschist to ultrahigh-pressure (UHP) eclogite facies, including the greenschist-facies Yingfeng dolerite dikes and basalts (846–821 Ma), the amphibolite- to HP granulite-facies Aolaoshan meta-volcanic sequence (protolith age of 832 Ma and metamorphic age of 439 Ma), and the North Qaidam UHP eclogites (protolith age of 847–828 Ma and metamorphic age of 440–420 Ma). Geochemical data reveal that they resemble present-day E-MORB/OIB and typical continental flood basalts. These features, together with high potential temperatures (T_p = 1434–1524 °C) for "primary" magmas, suggest that these basaltic rocks were most likely derived from a mantle plume source and were emplaced in a continental extensional environment.

Their varying metamorphic facies record a range of locations along the underthrust continental slab from near-surface (Yingfeng dolerites/basalts), middle (Aolaoshan amphibolites) to deep (N. Qaidam UHP eclogites) sites with depths greater than 120 km. The large spatial distribution (potentially >0.1 Mkm^2), short duration (<30 Myr) and intraplate geochemical character suggest that these igneous rocks are remnants of the North Qaidam LIP caused by the upwelling of a mantle plume during 850–820 Ma. We consider that the North Qaidam LIP represents the onset of a protracted break-up history and precedes subsequent multiple episodes of rifting. These Neoproterozoic igneous rocks in the Qaidam block were separated from the contemporaneous magmatic suites over Australia, South China and Tarim by the breakup of Rodinia, and were further destroyed by the subduction of the passive continental margin of the Qaidam block in the Early Paleozoic (440–420 Ma).

1. Introduction

Large Igneous Provinces (LIPs) are exceptional intraplate igneous events that represent massive crustal emplacement of mafic magmas, generated by processes distinct from normal seafloor spreading and plate convergence (Coffin and Eldholm, 1994; Ernst et al., 2005; Ernst and Jowitt, 2013; Ernst, 2014). Both continental and oceanic LIPs are likely to result from mantle plume heads arriving at the base of lithosphere, and are characterized by their large volume (at least 100,000 km^3), short duration (or short duration pulses), and geochemical and/or other affinities consistent with an intraplate tectonic setting (e.g., Richards et al., 1989; Coffin and Eldholm, 1994; Saunders, 2005; Bryan and Ernst, 2008; Ernst et al., 2008; Garfunkel, 2008; Bryan and Ferrari, 2013; Ernst, 2014). Most continental LIPs are dominated by flood basalts or their erosional/deformational remnants, a plumbing system of dikes and sills, and mafic–ultramafic layered

* Corresponding author.
E-mail address: sgsong@pku.edu.cn (S. Song).

http://dx.doi.org/10.1016/j.precamres.2016.07.007
0301-9268/

intrusions (e.g., Bryan and Ernst, 2008). A substantial silicic component may be present in some cases, for example Sierra Madre Occidental (e.g., Bryan and Ferrari, 2013). Thick outpourings of flood basalts have been identified on rifted continental margins around the world and are closely connected with the onset of seafloor spreading (e.g., the Greenland traps and North Atlantic Igneous Province for the opening of the North Atlantic, the Deccan traps for the Indian Ocean, and the Paraná–Etendeka traps for the South Atlantic; White and McKenzie, 1989; Courtillot et al., 1999; Bryan and Ernst, 2008). Thus it is proposed that there are causal links between the formation of ancient LIPs and the growth, breakup and cycles of supercontinents, and they are critical for recognizing the episodes of continental breakup and constraining supercontinental reconstructions (White and McKenzie, 1989; Hill et al., 1992; Park et al., 1995; Saunders et al., 1996; Wingate et al., 1998; Courtillot et al., 1999; Li et al., 1999, 2008a; Ernst et al., 2005, 2008; Ernst and Jowitt, 2013).

In the last decades, the amalgamation, breakup and configuration of Rodinia have attracted much attention (e.g. Li et al., 2008a and references herein). It is widely accepted that the assembly of this supercontinent is associated with the worldwide Grenville-age orogeny (1.3–0.9 Ga) which has been recognized within North America, Scandinavia, Australia, South China, India, East Antarctica, Tarim and in the Qilian–Qaidam area (Li et al., 2008a; Song et al., 2012). However, the timing of the onset of the prolonged breakup process has been controversial. The first episode of Neoproterozoic plume activity was identified in light of the ca. 825 Ma mafic dikes and sills, komatiites, mafic–ultramafic intrusions, continental flood basalts (CFBs), and anorogenic granitoids in South China, Tarim and Australia (see Li et al. (2008a) for details). These magmatic events are also correlated to the initial rift phase of the Nanhua rift basin in South China and the Adelaide geosyncline in southeastern Australia (Powell et al., 1994; Preiss, 2000; Wang and Li, 2003; Li et al., 2003a). However, recent geochronological results suggest that the intraplate magmatism related to the breakup of Rodinia may have started earlier, perhaps at 870–850 Ma in South China, Qilian–Qaidam, Africa, India, Australia, the Scottish promontory of Laurentia and the Scandinavian Caledonides (Song et al., 2010 and references therein) or even at ca. 930 Ma in North China and West Africa (Peng et al., 2011; Ernst, 2014). Alternatively, Zhou et al. (2002, 2006a,b) and Wang et al. (2007) speculated that the magmatism of this period was formed in an active continental margin or a collisional orogen around the Yangtze Craton.

It is generally considered that the Qilian–Qaidam block was an integral component of Rodinia, and had a close relationship with South China (Xu et al., 2015 and references herein). In terms of the Grenville-age magmatism and metamorphism, Song et al. (2012) identified the link between the South China, Qilian–Qaidam and Tarim blocks, and named them as the "South-West China United Continent" (Fig. 1a). Nevertheless, the process of separation away from the rest of Rodinia for the Qilian–Qaidam block is still poorly understood due to the sparse intraplate magmatic records, not least because of later fragmentation, erosion, burial and metamorphism related to the Early Paleozoic collisional orogeny.

The North Qaidam ultrahigh-pressure metamorphic (UHPM) belt on the northern Tibetan Plateau is a continental subduction/-collisional suture, where the ancient passive continental margin of the Qaidam block was dragged to depths greater than 100 km and was destroyed during the period of 440–420 Ma (Song et al., 2006, 2012, 2014). However, the protoliths of eclogites in the North Qaidam UHPM belt have been controversial, as to whether they represent oceanic crust or continental basalts, which is significant for understanding the tectonic evolution from oceanic subduction to continental subduction-collision (Song et al., 2014 and references therein).

In this paper, we present petrological, geochronological, geochemical and Sm-Nd isotopic data for the Yingfeng dolerite dikes/basalts and the Aolaoshan meta-volcanic rocks in the western extension of the North Qaidam UHPM belt. By combining our data with the previous results on the North Qaidam eclogites and neighboring mafic–ultramafic intrusions, we suggest that these igneous rocks form in the within-plate environment with a mantle plume origin and are remnants of the 850–820 Ma North Qaidam LIP, associated with the initial breakup of Rodinia.

2. Geological setting

The Qaidam block in the northern margin of Qinghai-Tibet Plateau is located between the larger South China, Tarim and North China blocks (Fig. 1a) and is covered with Mesozoic to Cenozoic sedimentary sequences. To its north, the North Qaidam continental-type ultra-high pressure metamorphic (UHPM) belt has a NW-SE trend, and is offset about 400 km by the left-lateral Altyn Tagh Fault. The Quanji block is separated from the North Qaidam UHPM belt by the Wulan-Yuka Fault (Zhang et al., 2001; Li et al., 2003b; Chen et al., 2007, 2009a). This block consists of Archean to Early Proterozoic gneisses, amphibolites and granulites, and is unconformably covered by the less deformed and metamorphosed Neoproterozoic Quanji Group and Cambrian-Ordovician sequences (see Chen et al., 2009a; Fig. 1b). The Qilian block in the north contains Precambrian basement rocks formed from Archean to Neoproterozoic with Grenville-age (1000–900 Ma) intrusions, and has a close affinity with the Yangtze block (Wan et al., 2001, 2006; Lu et al., 2008; Song et al., 2013). Recent studies suggested that the combined Qilian–Qaidam microcontinent was a fragment of the Rodinia supercontinent, and rifted away from southeastern Australia at 600–550 Ma (Xu et al., 2015). Further to the north is the North Qilian oceanic suture zone, which consists of ophiolites, arc volcanic rocks and lawsonite-bearing eclogites and blueschists associated with the oceanic subduction in the Early Paleozoic era (see Song et al., 2013 for details).

The North Qaidam UHPM belt extends discontinuously for over 400 km from Dulan in the southeast, northwestward through Xitieshan and Lüliangshan to Yuka (see Fig. 1b for localities). The lithologies mainly consist of granitic and pelitic gneisses (~80%) with eclogite and garnet peridotite blocks. The granitic and pelitic gneisses recorded a Grenville-age orogenesis at ~1020–900 Ma (Wan et al., 2006; Song et al., 2012, 2014; Zhang et al., 2012, 2015; Yu et al., 2013). Coesite and diamond inclusions have been identified in zircons and garnets from the metapelites, eclogites and garnet peridotites, which suggest that the UHP metamorphism occurred at depths of 100–200 km at 438–420 Ma (Song et al., 2014 and references therein).

3. Occurrence and petrography

Three types/occurrences of the 850–820 Ma volcanic rocks were identified in the North Qaidam region as following: (1) Yingfeng low-grade meta-mafic dikes/basalts, (2) Aolaoshan medium-grade meta-volcanics and (3) eclogite blocks in the North Qaidam UHPM belt associated with continental subduction.

3.1. Yingfeng low-grade meta-mafic dikes/basalts

The Yingfeng mafic dikes and basalts (Site 5 in Fig. 1a) are located at the northwest of the Yuka eclogite-gneiss terrane (Fig. 1b). The Yingfeng mafic rocks mainly occur as sills, dikes and layered basalts (Fig. 2a-b). The dikes dominantly trend in a NW-direction, with lengths ranging from 1 to 3 km and widths from 2 to 5 m. Together with large sills (1 × 5 km), they intrude

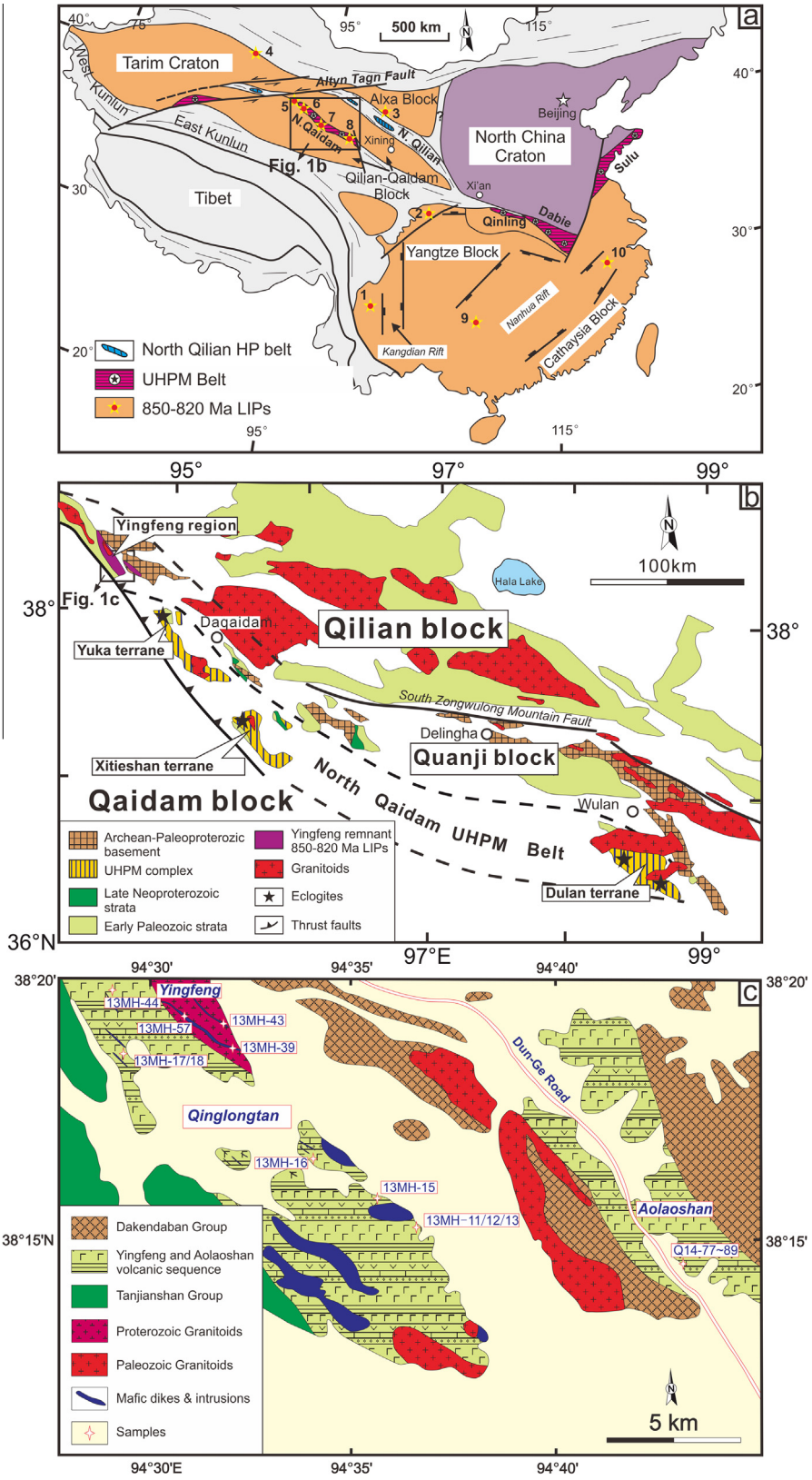

Fig. 1. (a) Tectonic framework of continental China showing the distribution of the 850–820 Ma LIP records throughout the inferred South-West China United Continent, involving the South China, Tarim, Qilian-Qaidam blocks (modified by Song et al., 2012). 1: 825–842 Ma Gaojiacun mafic-ultramafic complexes (Zhu et al., 2006); 2: 821 Ma Bikou basalts (Wang et al., 2008); 3: 828 Ma Jinchuan mafic-ultramafic intrusions (Li et al., 2005); 4: 824 Ma Quruqtagh dolerites dikes (Zhang et al., 2009); 5: 820–850 Ma Yingfeng–Aolaoshan dolerite dikes and flood basalts (Lu et al., 2008; this study); 6: 847 Ma CFB protolith of Yuka eclogites (Song et al., 2010); 7: 877 Ma protolith of Xitieshan eclogites (Zhang et al., 2011, 2012); 8: 828–838 Ma protolith of Dulan eclogites (Zhang et al., 2010; Yu et al., 2013); 9: 828 Ma mafic to ultramafic dikes and sills of North Guangxi (Li et al., 1999); 10:~850 Ma Zhenzhushan bimodal volcanic rocks, Wuyi basalts/gabbros, Gangbian alkaline complex and Shenwu dolerite dikes (Li et al., 2008b, 2010a,b; Shu et al., 2011). (b) Geological map of the North Qaidam ultra-high pressure metamorphic (UHPM) belt. (c) Geological sketch map of the Yingfeng and Aolaoshan regions with sample locations.

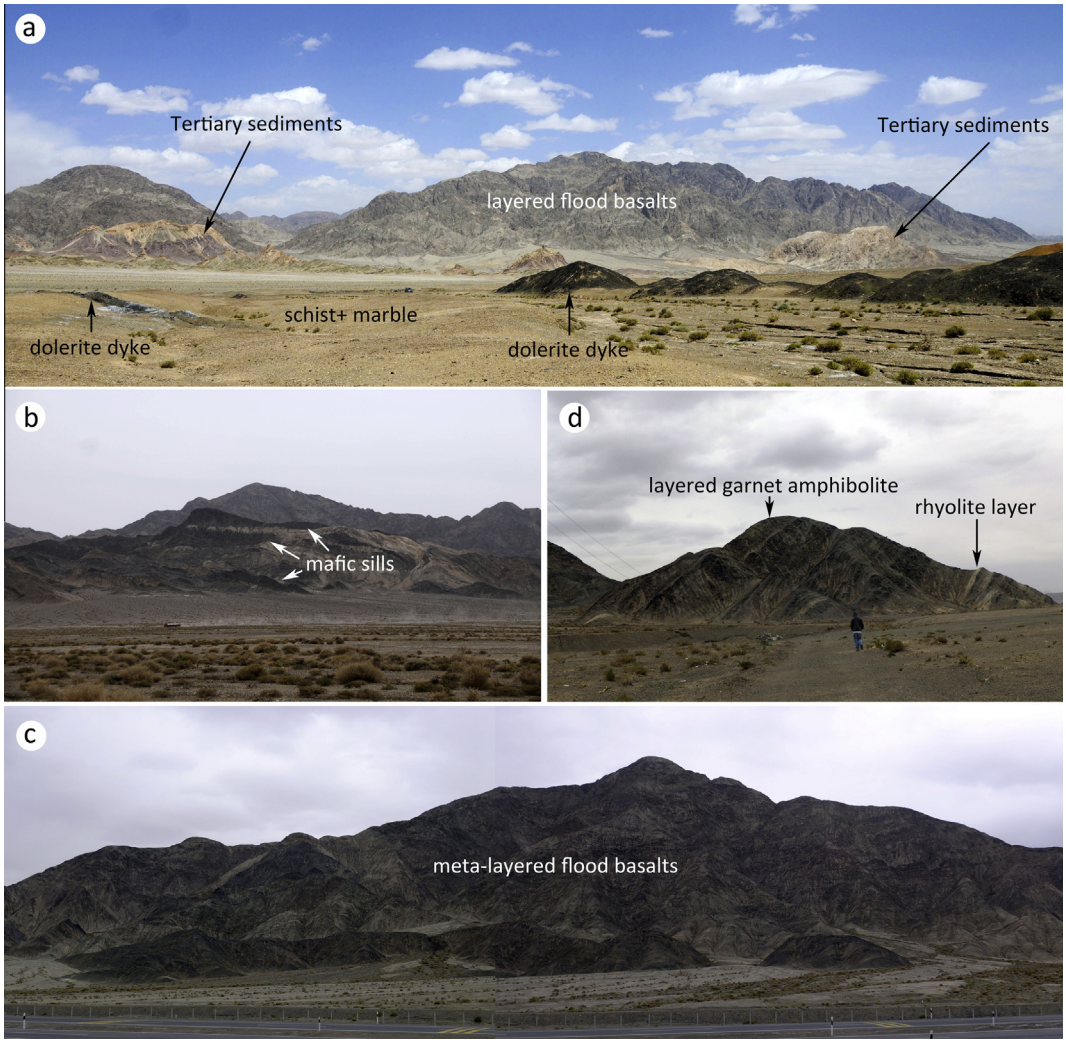

Fig. 2. Photographs showing occurrences of the Yingfeng–Aolaoshan mafic rocks. (a) Dolerite dikes and flood basalts (~845 Ma) in the Yingfeng area. (b) Mafic sills interbedded with marble-schist in the Yingfeng area. (c) Thick sequence of flood basalts in the Aolaoshan area. (d) Layered amphibolites with two rhyolite interlayers (~832 Ma) in the Aolaoshan area.

into the meta-sedimentary strata (schist + marble + phyllite) and a Mesoproterozoic rapakivi granitic pluton (Xiao et al., 2003; Fig. 1c). However, the flood basalts occur as thick lava layers (~100 m) with small amounts of sedimentary intercalations. The mafic dikes and sills show medium- to coarse-grained ophitic/gabbro texture in thin sections (Fig. 3a-b). They mainly consist of 30–35% plagioclase, 55–60% pyroxene and a minor amount of Fe-Ti oxides, sphene and calcite. Most pyroxene was replaced by amphibole, chlorite or epidote. Euhedral plagioclase underwent variable degrees of saussuritization and epidotization, suggesting greenschist facies metamorphism. The basalts have a fine-grained pilotaxitic texture with plagioclase laths and altered groundmass replaced by amphibole and epidote (Fig. 3c).

3.2. Aolaoshan medium-grade meta-volcanics

The Aolaoshan meta-volcanic sequence (Site 5 in Fig. 1a) mainly consists of thick meta-basaltic layers (100–200 m) with rare sedimentary interlayers (Fig. 2c). Thin meta-rhyolite interlayers (white-colored) are occasionally present (Fig. 2d). The mafic rocks underwent amphibolite- to high-pressure granulite facies metamorphism. The analytical method for mineral chemistry and the representative mineral compositions used for *P–T* calculations are given in Appendix Table 1. The garnet amphibolite (Q14-87) is chiefly composed of plagioclase, hornblende, garnet and quartz with minor clinopyroxene and biotite (Fig. 3e-f). Rutile occurs as inclusions in garnet. Clinopyroxene occurs as fine-grained crystals around coarse amphibole, suggesting a prograde metamorphism. Application of the garnet-clinopyroxene geothermometer (Ravna, 2000) together with garnet-clinopyroxene-plagioclase-quartz geobarometer (Eckert et al., 1991) give the metamorphic peak condition of $P = 17–19$ kbar and $T = 728–825$ °C. The amphibolite (Q14-88) mainly consists of hornblende, plagioclase with minor garnet (Fig. 3d). Garnet-hornblende-plagioclase-quartz thermobarometry (Holland and Blundy, 1994; Dale et al., 2000) yields the *P–T* conditions of 705–727 °C and 10–11 kbar.

3.3. Eclogite blocks in N. Qaidam UHPM belt

Eclogites in the three terranes of the North Qaidam UHPM belt (Site 6–8 in Fig. 1a) mainly occur as various sized blocks, layers and boudinaged dikes within granitic and pelitic gneisses. Two types of protoliths of these eclogite blocks have been identified: (1) the Cambrian ophiolite with protolith ages of ~540–500 Ma (Zhang et al., 2008; Song et al., 2009), and (2) Neoproterozoic CFB with protolith ages of 850–820 Ma (Chen et al., 2009; Song et al.,

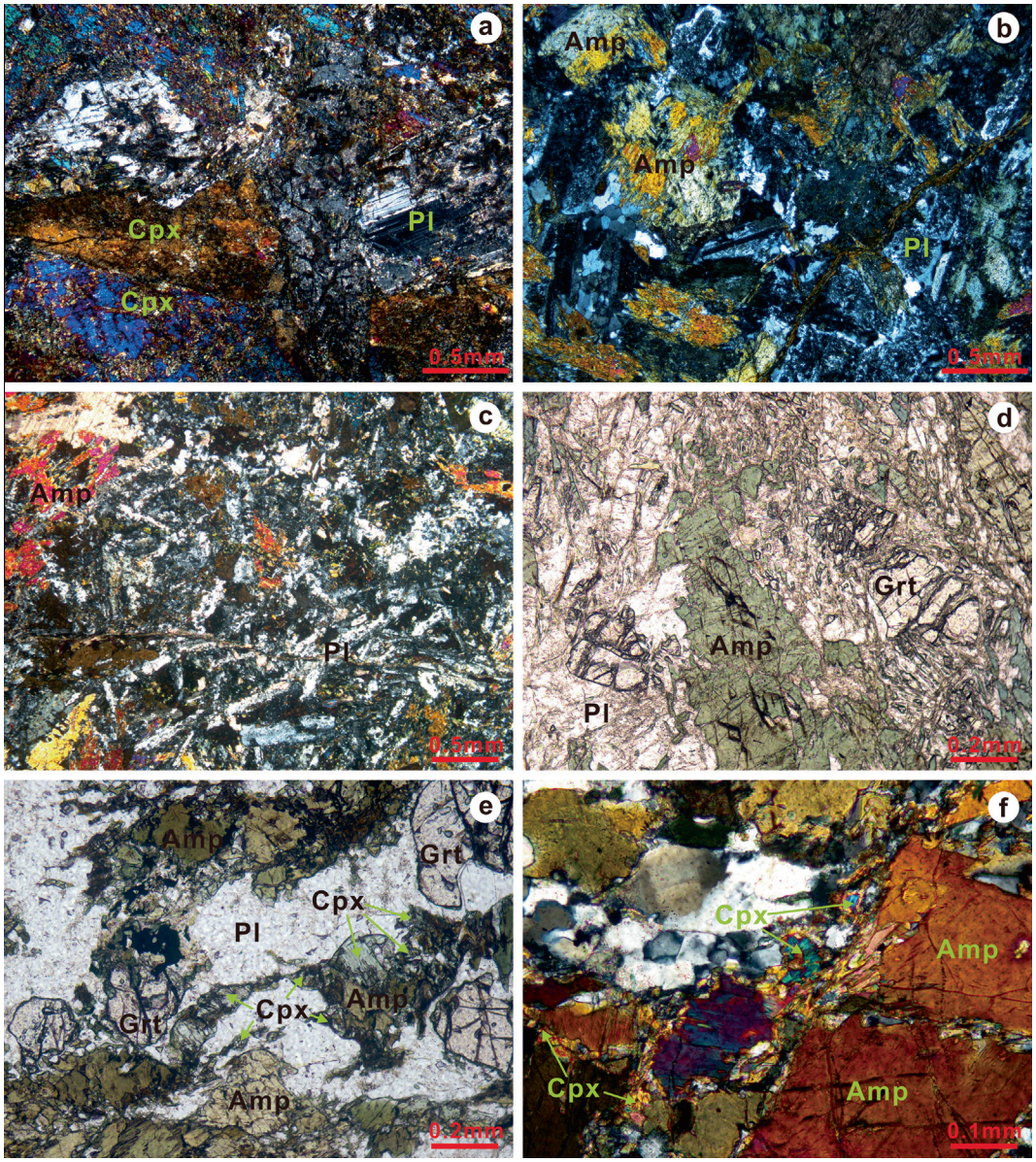

Fig. 3. Photomicrographs showing textures of the Yingfeng dolerite dikes/basalts, and the Aolaoshan meta-mafic rocks. (a) Yingfeng dolerite dike with coarse-grained gabbroic texture (13MH-13). (b) Yingfeng dolerite dike with medium-grained ophitic texture (13MH-15). (c) Yingfeng basalt with fine-grained pilotaxitic texture (13MH-44). (d) Aolaoshan amphibolite with minor garnet porphyroblasts (Q14-88). (e) Aolaoshan garnet amphibolite (Q14-87). (f) Fine-grained clinopyroxene growing around amphibole (Q14-87).

2010; Zhang et al., 2010, 2015). The peak metamorphic *P–T* conditions for both types of eclogites have been estimated in ranges of $P = 2.6–3.5$ GPa and $T = 600–830$ °C, and zircons from these eclogites yielded HP-UHP metamorphic ages ranging from 470 Ma to 420 Ma, indicating a complete orogenic process from oceanic subduction to continental collision (Song et al., 2014 and references herein).

The CFB-type eclogites with protolith ages of 850–820 Ma in Yuka terrane have been descripted by Song et al. (2010), while those occurred in the Xitieshan and Dulan terranes are shown in Fig. 4. They all occur in large blocks intercalated with granitic and pelitic gneisses. Some eclogite layers are several to tens of meters in thickness and extend for more than 1 km. Most eclogites are fresh, show a medium- to coarse-grained granular texture and have a typical mineral assemblage of garnet, omphacite, rutile and phengite.

4. Analytical methods

4.1. In situ zircon U-Pb dating

Zircons were separated by heavy liquid and magnetic techniques. These grains were enclosed in epoxy resin and polished to half of their thickness. The grain mount was imaged in reflected and transmitted light as well as cathodoluminescence (CL) in order to select analysis positions. The CL examination was conducted by a Scanning Electron Microscope (SEM) at Peking University. The grain mount was vacuum-coated with high-purity gold before secondary ion mass spectroscopy (SIMS) U-Pb isotope analyses.

U, Th and Pb isotopic compositions for sample 13MH-18 were analyzed using the Cameca IMS-1280 SIMS at the Institute of Geology and Geophysics, Chinese Academy of Sciences. The instrument description and analytical procedure are given in Li et al.

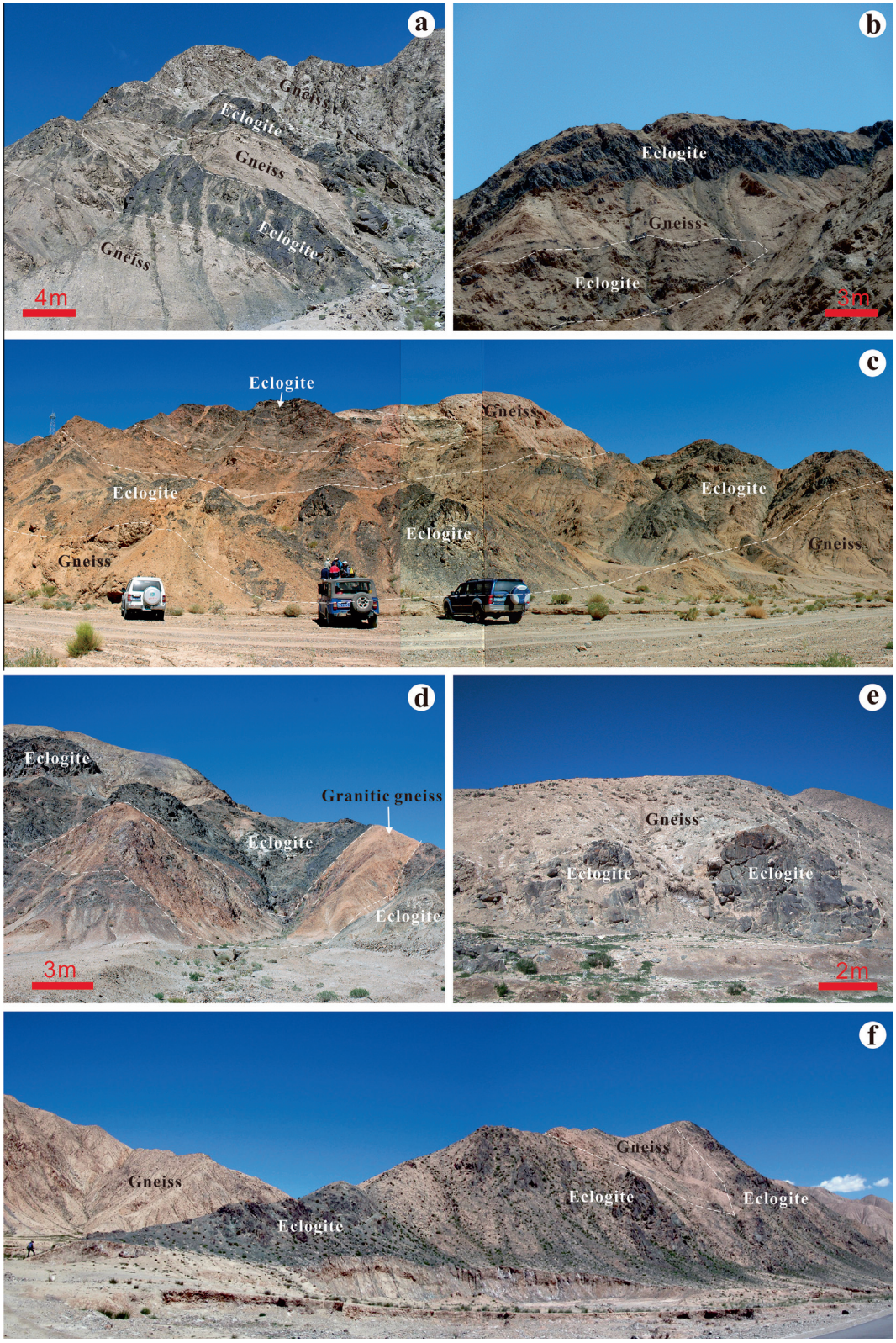

Fig. 4. Field photographs and occurrences of eclogites in the North Qaidam UHPM belt. (a and b) Layered eclogite blocks in the Yuka terrane. (c and d) Layered eclogite blocks in the Xitieshan terrane. (e and f) Large eclogite blocks in the Dulan terrane.

(2009). U-Th-Pb ratios were determined relative to the standard zircon Plešovice (Sláma et al., 2008) and their absolute abundances were calibrated to standard zircon 91500 (Wiedenbeck et al., 1995). Analyses of the Plešovice standard were interspersed with those of unknown grains. A long-term uncertainty of 1.5% (1σ) for $^{206}Pb/^{238}U$ measurements of the standard zircons was propagated to the unknowns (Li et al., 2010c), despite that the measured $^{206}Pb/^{238}U$ error in a specific session is generally 1% (1σ).

Correction of common lead was made by measuring non-radiogenic ^{204}Pb. An average Pb of present-day crustal composition (Stacey and Kramers, 1975) was used for the common Pb, assuming that it was largely due to surface contamination introduced during sample preparation. In order to monitor the external uncertainties, the standard Qinghu was alternately analyzed together with other unknown zircons. Seven measurements on the Qinghu zircons for SIMS analyses yield a concordia age of 160.6 ± 0.9 Ma (MSWD = 0.54), which is identical within error to the recommended value of 159.5 ± 0.2 Ma (Li et al., 2013).

Measurements of U-Th-Pb isotopes for sample 13MH-19, 13MH-44, and Q14-77 were carried out on an Agilent-7500a quadrupole inductively coupled plasma-mass spectrometry coupled with a New Wave SS UP193 laser sampler (LA-ICP-MS) at the Geological Lab Center, China University of Geosciences, Beijing (CUGB). A laser spot size of 36 μm, a laser energy density of 8.5 J/cm^2, and a repetition rate of 10 Hz were applied for analysis. National Institute of Standards and Technology 610 glass and Harvard zircon 91500 (Wiedenbeck et al., 1995) were used as external standards, Si as an internal standard, and zircon standard TEMORA (417 Ma) from Australia (Black et al., 2003) as the secondary standard. The common lead correction was done following Andersen (2002). Analytical details are described in Song et al. (2010). The standard Qinghu zircons give a concordia age of 162.0 ± 0.6 Ma (n = 10, MSWD = 1.4).

Data processing was carried out using the Isoplot/Ex v. 2.49 program (Ludwig, 2001). Uncertainties on individual analyses in the data tables are reported at 1σ level. The weighted mean $^{206}Pb/^{238}U$ ages are quoted with 95% confidence interval. The Qinghu zircon data for SIMS and LA-ICP-MS are provided in Appendix Table 2.

4.2. Bulk rock major and trace element analyses

The bulk-rock major and trace elements were analyzed at CUGB. Major elements were analyzed using a Leeman Prodigy inductively coupled plasma-optical emission spectroscopy (ICP-OES) instrument with high-dispersion Echelle optics. Based on rock standards AGV-2, GRS-1, and GSR-3 (national geological standard reference material of China), the analytical precisions (1σ) for most major elements (Appendix Table 3) are better than 1% with the exception of TiO_2 (~1.5%) and P_2O_5 (~2.0%). Loss on ignition was determined by placing 1 g of samples in the furnace at 1000 °C for several hours before being cooled in a desiccator and reweighed.

Bulk rock trace element analysis was done on an Agilent-7500a inductively coupled plasma-mass spectrometry (ICP-MS) instrument. Roughly 40 mg of sample powder was dissolved in an equal mixture of subboiling distilled HNO_3 and HF with a Teflon digesting vessel on a hot plate at 285 °C for 48 h using high-pressure bombs to aid digestion/dissolution. The samples were then evaporated to incipient dryness, refluxed with 6 N HNO_3, and heated again to incipient dryness. They were then dissolved in 2 ml of 3 N HNO_3 using high-pressure bombs for a further 24 h to ensure complete digestion/dissolution. After digestion, they were diluted with Milli-Q water (18 MΩ) to a final dilution factor of 2000. Rock standards AGV-2 and GSR-3 were used to monitor the analytical accuracy and precision (Appendix Table 4). Analytical accuracy, as indicated by relative difference between measured and recommended values, is better than 5% for most elements, and better than 10 ~ 15% for Gd and Ta.

4.3. Bulk rock Sr-Nd isotope analyses

The separation and determination of Sm-Nd isotopes were carried out at the Ministry of Education (MOE) Key Laboratory of Orogenic Belts and Crustal Evolution, Peking University. Powders of samples (~300 mg) and standard BCR-2 (~200 mg) were dissolved by using HF + HNO_3 in sealed Teflon capsules and heated on a hot plate for 7 days. REEs were separated using AG50 W cation-exchange columns. Sm and Nd were further purified by passing REE through second P507 cation-exchange columns, conditioned and eluted with dilute HCl. Sm–Nd isotopic compositions were measured by a VG-AXIOM HR-MC-ICP-MS. Each sample was analyzed in between two determination of the standard solutions (JNdi for Nd). The $^{147}Sm/^{144}Nd$ ratios were calculated from Sm and Nd contents measured by ICP–MS. The measured $^{143}Nd/^{144}Nd$ ratios have been normalized to $^{146}Nd/^{144}Nd$ = 0.7219, and adjusted to JNdi standard = 0.512120. In order to monitor the accuracy and reliability data, the standard BCR-2 was also analyzed together with unknown samples. Four measurements yielded $^{143}Nd/^{144}Nd$ = 0.512622 ± 14, 0.512624 ± 20, 0.512622 ± 14 and 0.512622 ± 11, which are within error of measurements reported by Weis et al. (2006).

5. Results

5.1. Zircon U-Pb ages

Sample 13MH-18 was collected from a dolerite dike in the Yingfeng region (see locality in Fig. 1c). Zircons selected for SIMS analyses are mostly irregular, tabular and transparent, and have length to width ratios up to 4:1. The results of SIMS U-Pb analyses are listed in Table 1. Twenty spots of 20 zircons were analyzed and show variable abundance of Th (180–906 ppm), U (196–838 ppm) and high Th/U (0.7–1.2). The common Pb content is low with mostly f_{206} < 0.1%. All apparent $^{206}Pb/^{238}U$ ages (824–873 Ma) are concordant within analytical errors and yield a weighted mean age of 845 ± 6 Ma (MSWD = 1.19). This age is comparable with the concordia age of 844 ± 2 Ma (MSWD = 0.26; Fig. 5a). CL images show uniform wide and straight oscillatory zones, and no cores are observed, which is typical for zircons that crystallize from mafic magma (Fig. 5a). Most grains are characterized by a narrow, highly luminescent rim, responding to a later regional thermal event.

Zircons from the dolerite samples (13MH-19 and 13MH-44) also have irregular or fragmented tabular shapes. CL investigations reveal that most grains contain a CL-dark or weak straight oscillatory domain surrounded by a narrow CL-bright overgrowth, which is similar to that of 13MH-18 (Fig. 5b-c). The results of LA-ICP-MS U-Pb analyses are given in Table 2. Twenty spots of 13MH-19 were determined with high Th/U ratios (0.9–1.8). Among these, 19 analyses have consistent apparent $^{206}Pb/^{238}U$ ages of 832–855 Ma and yield a weighted mean age of 851 ± 5 Ma (MSWD = 0.35), which is consistent with the concordia age of 852 ± 2 Ma (MSWD = 1.2; Fig. 5b). Another zircon grain gives distinctly older $^{206}Pb/^{238}U$ age (981 ± 11 Ma), indicating that it may be captured from the basement rocks. A total of 10 spots were analyzed on 10 grains for 13MH-44. The apparent $^{206}Pb/^{238}U$ ages range from 830 Ma to 858 Ma and yield a mean age of 846 ± 6 Ma (MSWD = 1.13; Fig. 5c). These spots are characterized by high Th/U ratios (1.9–4.1). However, some spots are slightly discordant perhaps due to Pb-loss during later metamorphism or deformation. Recently, Lu et al. (2008) also reported a SHRIMP U-Pb age of 821 ± 11 Ma for these mafic dikes. Thus we conclude that Yingfeng dolerite dikes and basalts formed at 820–850 Ma.

The Aolaoshan meta-rhyolite (Q14-77) is interbedded with meta-basalt layers (Fig. 2d). The results of LA-ICP-MS U-Pb analyses are listed in Table 2. The zircons are colorless and subhedral-euhedral with 100–200 um in length and 50–100 um in width. Cathodoluminescence (CL) investigations reveal that a few zircon grains contain a CL-bright, oscillatory zoned core surrounded by

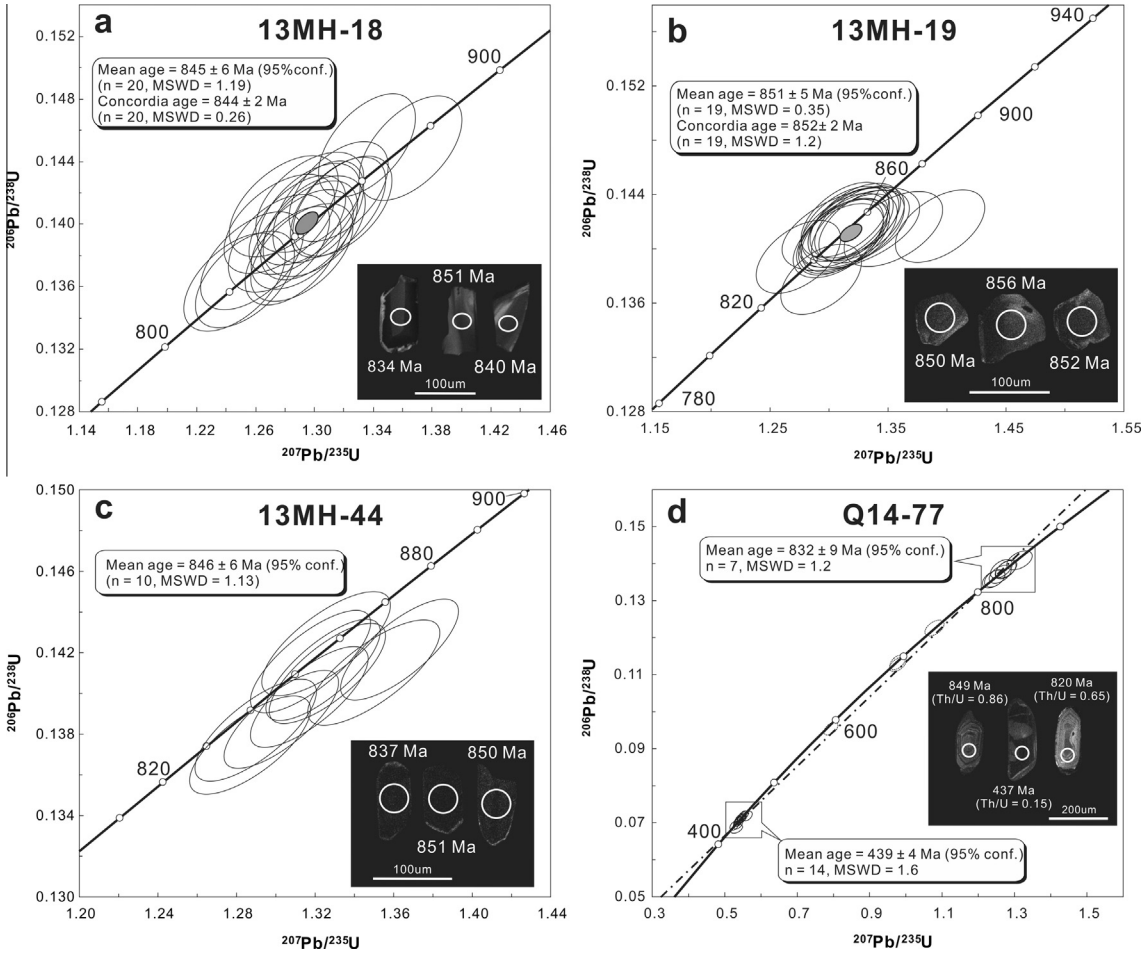

Fig. 5. (a) U-Pb concordia diagram for SIMS analyses of the Yingfeng dolerite (13MH-18). (b-c) U-Pb concordia diagram for LA-ICP-MS analyses of the Yingfeng dolerite (13MH-19 and 13MH-44). (d) U-Pb concordia diagram for LA-ICP-MS analyses of the Aolaoshan meta-rhyolite (Q14-77).

Table 1
In-situ SIMS zircon U-Pb data for the Yingfeng dolerite (13MH-18).

Sample spot #	U ppm	Th ppm	$\frac{Th}{U}$	f_{206} (%)	$\frac{^{207}Pb}{^{206}Pb}$	±1σ (%)	$\frac{^{207}Pb}{^{235}U}$	±1σ (%)	$\frac{^{206}Pb}{^{238}U}$	±1σ (%)	Age 207/206 (Ma)	±1σ	Age 207/235 (Ma)	±1σ	Age 206/238 (Ma)	±1σ
13MH-18																
1	526	617	1.17	0.27	0.0684	0.75	1.365	1.68	0.1448	1.51	880	15	874	10	872	12
2	288	200	0.69	0.00	0.0678	0.91	1.292	1.76	0.1382	1.50	862	19	842	10	834	12
3	196	180	0.92	0.03	0.0657	1.13	1.280	1.88	0.1412	1.51	798	24	837	11	851	12
4	421	426	1.01	0.03	0.0667	0.92	1.276	1.76	0.1387	1.50	828	19	835	10	838	12
5	299	283	0.95	0.08	0.0663	1.00	1.246	1.81	0.1363	1.50	816	21	822	10	824	12
6	300	320	1.07	0.10	0.0663	1.04	1.258	1.83	0.1377	1.50	815	22	827	10	831	12
7	785	868	1.11	0.01	0.0674	0.64	1.296	1.63	0.1396	1.50	849	13	844	9	842	12
8	259	269	1.04	0.00	0.0674	0.96	1.300	1.78	0.1398	1.50	851	20	846	10	844	12
9	468	504	1.08	0.00	0.0676	0.73	1.286	1.68	0.1380	1.51	856	15	840	10	833	12
10	284	256	0.90	0.07	0.0669	0.94	1.296	1.77	0.1406	1.50	833	19	844	10	848	12
11	406	375	0.92	0.03	0.0666	0.91	1.253	1.75	0.1364	1.50	825	19	825	10	824	12
12	508	600	1.18	0.03	0.0672	0.68	1.317	1.65	0.1421	1.50	844	14	853	10	856	12
13	396	438	1.10	0.09	0.0674	0.96	1.292	1.79	0.1390	1.51	851	20	842	10	839	12
14	662	687	1.04	0.03	0.0668	0.62	1.336	1.62	0.1450	1.50	831	13	861	9	873	12
15	389	341	0.88	0.00	0.0668	0.79	1.289	1.70	0.1399	1.50	832	16	841	10	844	12
16	351	337	0.96	0.04	0.0665	1.14	1.297	1.89	0.1414	1.50	823	24	844	11	852	12
17	233	229	0.98	0.06	0.0661	1.20	1.276	1.92	0.1400	1.50	810	25	835	11	845	12
18	402	492	1.22	0.00	0.0678	0.78	1.320	1.69	0.1412	1.50	862	16	854	10	851	12
19	838	906	1.08	0.01	0.0672	0.54	1.303	1.59	0.1407	1.50	843	11	847	9	849	12
20	826	876	1.06	0.00	0.0677	0.54	1.317	1.59	0.1411	1.50	859	11	853	9	851	12

f_{206} is the percentage of common ^{206}Pb in total ^{206}Pb.

Table 2
In-situ LA-ICP-MS zircon U-Pb data for the Yingfeng dolerites (13MH-19 and 13MH-44) and the Aolaoshan meta-rhyolite (Q14-77).

Spot #	Concentration (ppm)		Th/U	Isotopic ratios						Age (Ma)					
	U	Th		$^{207}Pb/^{206}Pb$	±1σ	$^{207}Pb/^{235}U$	±1σ	$^{206}Pb/^{238}U$	±1σ	$^{207}Pb/^{206}Pb$	±1σ	$^{207}Pb/^{235}U$	±1σ	$^{206}Pb/^{238}U$	±1σ
13MH-19															
1	386	482	1.25	0.06739	0.00119	1.31811	0.02358	0.14183	0.00174	850	18	854	10	855	10
2	259	287	1.11	0.06737	0.00126	1.30901	0.02451	0.14089	0.00176	849	20	850	11	850	10
3	532	818	1.54	0.07210	0.00123	1.63458	0.02825	0.16439	0.00200	989	17	984	11	981	11
4	222	227	1.02	0.06703	0.00125	1.31381	0.02462	0.14212	0.00177	839	20	852	11	857	10
5	600	938	1.56	0.06794	0.00119	1.32727	0.02354	0.14166	0.00173	867	18	858	10	854	10
6	145	224	1.54	0.06938	0.00148	1.35383	0.02860	0.14149	0.00184	910	23	869	12	853	10
7	520	642	1.23	0.06783	0.00121	1.32173	0.02379	0.14129	0.00174	863	19	855	10	852	10
8	401	639	1.59	0.07137	0.00131	1.39430	0.02573	0.14165	0.00176	968	19	887	11	854	10
9	784	939	1.19	0.06807	0.00120	1.29315	0.02310	0.13776	0.00169	871	18	843	10	832	10
10	664	740	1.11	0.06748	0.00121	1.31264	0.02378	0.14105	0.00174	853	19	851	10	851	10
11	684	895	1.32	0.06722	0.00124	1.31438	0.02445	0.14179	0.00176	845	20	852	11	855	10
12	466	424	0.91	0.06730	0.00126	1.31217	0.02477	0.14138	0.00176	847	20	851	11	852	10
13	75	76	1.01	0.06764	0.00202	1.31945	0.03885	0.14144	0.00193	858	39	854	17	853	11
14	326	553	1.69	0.06756	0.00128	1.32114	0.02515	0.14179	0.00178	855	20	855	11	855	10
15	142	161	1.14	0.06780	0.00158	1.32225	0.03047	0.14141	0.00185	862	27	855	13	853	10
16	656	737	1.12	0.06752	0.00129	1.31249	0.02524	0.14095	0.00177	854	20	851	11	850	10
17	409	544	1.33	0.06742	0.00130	1.30758	0.02522	0.14063	0.00176	851	21	849	11	848	10
18	716	1302	1.82	0.06780	0.00126	1.32624	0.02488	0.14184	0.00176	862	20	857	11	855	10
19	367	434	1.18	0.06625	0.00127	1.27389	0.02452	0.13942	0.00175	814	21	834	11	841	10
20	579	658	1.14	0.06753	0.00129	1.32245	0.02534	0.14200	0.00178	854	20	856	11	856	10
13MH-44															
1	1806	6004	3.33	0.06955	0.00097	1.36335	0.01989	0.14214	0.00166	915	14	873	9	857	9
2	1783	3984	2.23	0.06811	0.00096	1.30278	0.01910	0.13870	0.00162	872	14	847	8	837	9
3	2587	10,639	4.11	0.06804	0.00096	1.32413	0.01943	0.14112	0.00165	870	14	856	8	851	9
4	1898	5724	3.02	0.06820	0.00096	1.32606	0.01947	0.14098	0.00165	875	14	857	8	850	9
5	1473	3888	2.64	0.06832	0.00098	1.31709	0.01958	0.13980	0.00164	878	14	853	9	844	9
6	1030	2316	2.25	0.06772	0.00103	1.29028	0.02029	0.13816	0.00164	860	15	841	9	834	9
7	1847	4394	2.38	0.06789	0.00103	1.28688	0.02006	0.13745	0.00163	865	15	840	9	830	9
8	2839	10,026	3.53	0.06752	0.00099	1.31794	0.02005	0.14154	0.00167	854	15	854	9	853	9
9	830	2227	2.68	0.06749	0.00106	1.32559	0.02139	0.14242	0.00170	853	16	857	9	858	10
10	914	1733	1.90	0.06942	0.00111	1.34996	0.02215	0.14100	0.00169	911	16	868	10	850	10
Q14-77															
1	1971	64	0.03	0.05569	0.00080	0.54595	0.00806	0.07109	0.00081	440	15	442	5	443	5
2	1524	147	0.10	0.05575	0.00082	0.54893	0.00830	0.07140	0.00082	442	16	444	5	445	5
3	959	228	0.24	0.06263	0.00093	0.97725	0.01484	0.11316	0.00130	696	15	692	8	691	8
4	756	319	0.42	0.06300	0.00096	0.97806	0.01525	0.11258	0.00130	708	16	693	8	688	8
5	656	347	0.53	0.06693	0.00099	1.27531	0.01924	0.13818	0.00159	836	15	835	9	834	9
6	2027	324	0.16	0.05561	0.00082	0.53928	0.00812	0.07032	0.00081	437	16	438	5	438	5
7	2494	84	0.03	0.05546	0.00081	0.52681	0.00791	0.06889	0.00079	431	16	430	5	429	5
8	3676	321	0.09	0.05599	0.00081	0.54755	0.00815	0.07092	0.00081	452	15	443	5	442	5
9	1664	190	0.11	0.05588	0.00083	0.55257	0.00841	0.07170	0.00083	448	16	447	6	446	5
10	351	302	0.86	0.06769	0.00118	1.31375	0.02302	0.14073	0.00168	859	18	852	10	849	9
11	1710	223	0.13	0.05565	0.00086	0.54160	0.00852	0.07058	0.00082	438	17	439	6	440	5
12	1613	165	0.10	0.05549	0.00114	0.54247	0.00929	0.07091	0.00081	432	47	440	6	442	5
13	2230	245	0.11	0.05569	0.00083	0.53785	0.00820	0.07003	0.00081	440	16	437	5	436	5
14	1795	204	0.11	0.05623	0.00085	0.53718	0.00834	0.06928	0.00080	461	16	437	6	432	5
15	261	171	0.65	0.06643	0.00109	1.24305	0.02057	0.13568	0.00160	820	17	820	9	820	9
16	2087	274	0.13	0.05668	0.00135	0.53219	0.01109	0.06810	0.00079	479	54	433	7	425	5
17	726	173	0.24	0.06045	0.00096	0.79385	0.01287	0.09523	0.00111	620	17	593	7	586	7
18	652	293	0.45	0.06679	0.00103	1.26111	0.01980	0.13692	0.00159	831	16	828	9	827	9
19	253	168	0.66	0.06660	0.00111	1.24940	0.02113	0.13603	0.00161	825	17	823	10	822	9
20	851	565	0.66	0.06694	0.00102	1.27779	0.01988	0.13842	0.00161	836	15	836	9	836	9
21	558	257	0.46	0.06400	0.00101	1.08010	0.01727	0.12239	0.00143	742	16	744	8	744	8
22	391	274	0.70	0.06621	0.00105	1.26346	0.02030	0.13838	0.00162	813	16	829	9	835	9
23	3571	575	0.16	0.05572	0.00083	0.54252	0.00830	0.07061	0.00082	441	16	440	5	440	5
24	2395	370	0.15	0.05565	0.00084	0.53777	0.00833	0.07007	0.00081	438	16	437	6	437	5
25	1161	124	0.11	0.05705	0.00089	0.56292	0.00894	0.07155	0.00083	493	17	453	6	445	5

a narrow CL-dark, structureless rim (Fig. 5d). However, most zircons have no cores and show inhomogeneous CL intensities with patchy, banded or structureless patterns, similar to that of rims surrounding inherited cores. A total of 25 spots were analyzed on 25 grains. All the data define a discordant line with an upper-intercept age of 803 ± 38 Ma and a lower-intercept age of 433 ± 18 Ma (Fig. 5d). Seven analyses from inherited cores yield $^{206}Pb/^{238}U$ ages of 820–849 Ma, combining to a mean age of 832 ± 9 Ma (MSWD = 1.2), which is consistent with the upper-intercept age. These spots are characterized by high Th/U ratios (0.45–0.86). However, 14 spots from the CL-dark domains give a mean $^{206}Pb/^{238}U$ age of 439 ± 4 Ma (MSWD = 1.6), which is indistinguishable with the lower-intercept age within error. They have low Th/U (0.03–0.16), indicating a metamorphic origin. Another four concordant U-Pb ages (586–744 Ma) are located between upper- and lower-intercept ages. The intermediate Th/U values (0.24–0.46) imply that they may represent mixed ages of core and rim domains. Therefore, we interpret that the weighted mean age of 832 ± 9 Ma represents the protolith age of Aolaoshan meta-volcanic rocks and the age of 439 ± 4 Ma represents the time

Table 3
Whole-rock major and trace element data for the Yingfeng dolerites/basalts and the Aolaoshan meta-volcanics.

Sample	Yingfeng dolerites/basalts										Aolaoshan meta-volcanics				
	13MH-11	13MH-12	13MH-13	13MH-15	13MH-18	13MH-35	13MH-43	13MH-44	13MH-57	13MH-67	Q14-85	Q14-87	Q14-89	Q14-83	Q14-84
Major elements (wt.%)															
SiO_2	50.28	50.86	49.67	45.29	48.29	51.25	50.38	44.77	44.09	48.81	42.55	46.75	47.30	70.96	69.29
TiO_2	1.00	1.04	0.90	1.80	0.96	1.03	1.17	1.74	1.20	1.06	1.24	0.85	0.75	0.06	0.05
Al_2O_3	13.62	13.52	12.85	17.07	12.36	12.91	14.27	16.78	17.39	13.44	16.09	18.09	19.26	15.05	15.77
Fe_2O_3T	11.88	11.84	13.30	14.70	10.53	11.78	12.67	14.29	13.57	11.08	13.37	11.27	11.96	0.45	0.42
MnO	0.19	0.18	0.19	0.20	0.16	0.20	0.20	0.21	0.21	0.16	0.20	0.19	0.24	0.01	0.01
MgO	7.42	6.89	9.72	6.68	11.22	7.62	6.70	6.77	7.81	9.27	9.42	7.26	6.55	0.18	0.14
CaO	11.38	10.94	9.78	9.73	11.20	8.17	9.52	12.55	10.81	11.89	11.72	8.56	5.96	1.99	1.83
Na_2O	1.93	1.39	2.07	2.83	1.51	1.03	3.02	2.14	2.56	1.90	2.75	4.88	5.77	2.28	2.27
K_2O	0.13	0.12	0.78	0.66	1.39	3.50	0.68	0.04	0.76	0.21	0.40	0.73	1.05	7.47	8.69
P_2O_5	0.07	0.07	0.14	0.20	0.07	0.09	0.11	0.18	0.11	0.08	0.06	0.12	0.12	0.03	0.03
LOI	1.3	2.3	1.4	1.3	1.7	1.6	1.7	1.2	1.7	1.4	1.5	0.6	0.3	0.8	0.9
Mg#	59.3	57.6	63.0	51.5	71.3	60.1	55.2	52.5	57.3	66.1	62.2	60.0	56.1	48.0	44.4
Total	99.20	99.16	100.76	100.45	99.40	99.20	100.41	100.65	100.22	99.32	99.35	99.25	99.26	99.23	99.38
Trace elements (ppm)															
Sc	52.7	52.5	6.4	42.6	52.8	48.9	19.7	37.2	41.3	52.0	41.8	37.6	36.9	0.7	0.5
V	358	372	243	391	293	330	315	353	335	327	314	323	305	4	3
Cr	263	200	137	183	600	239	139	59	204	496	305	383	177	2	4
Co	49	50	56	43	39	54	46	44	44	49	54	33	32	1	1
Ni	90	83	220	64	178	114	92	52	103	142	146	79	51	2	2
Rb	1.71	1.18	16.24	11.64	37.42	144.46	14.21	0.47	20.00	5.99	6.22	2.99	6.75	179.80	216.00
Sr	147	168	153	234	164	172	275	354	252	176	310	259	302	219	195
Y	20.9	22.2	15.5	29.2	18.2	20.9	20.1	26.2	22.7	20.6	20.4	24.9	20.6	4.1	2.7
Zr	62	67	58	133	61	70	73	111	67	67	56	69	50	101	51
Nb	3.6	3.9	3.3	15.2	5.5	3.9	5.3	9.1	3.9	6.2	3.0	1.0	1.2	1.3	0.6
Ba	31	13	189	120	153	1080	116	23	369	33	141	79	120	723	332
La	3.8	4.0	3.5	14.9	4.8	3.9	5.2	8.6	3.9	5.7	3.8	10.0	8.4	40.3	7.4
Ce	10.1	10.6	9.8	35.3	11.8	10.4	13.5	21.9	10.5	13.9	10.4	26.3	19.5	76.2	13.4
Pr	1.55	1.64	1.55	4.71	1.71	1.62	1.97	3.12	1.62	2.00	1.64	3.70	2.71	8.30	1.45
Nd	7.5	8.0	7.6	19.5	7.9	7.9	9.1	14.0	7.9	9.1	8.1	16.4	12.0	26.6	4.9
Sm	2.41	2.54	2.41	4.88	2.35	2.54	2.77	4.02	2.60	2.65	2.63	3.86	2.99	4.07	0.94
Eu	0.94	1.01	0.93	1.73	0.83	1.09	1.06	1.43	1.03	1.02	1.06	1.09	0.94	1.00	0.65
Gd	3.17	3.37	3.04	5.39	2.97	3.30	3.46	4.70	3.44	3.32	3.38	3.90	3.15	2.66	0.78
Tb	0.573	0.610	0.526	0.898	0.522	0.585	0.613	0.802	0.631	0.582	0.609	0.664	0.533	0.277	0.108
Dy	3.73	3.92	3.23	5.38	3.31	3.73	3.84	4.88	4.02	3.68	3.81	4.25	3.40	1.04	0.55
Ho	0.799	0.841	0.697	1.141	0.692	0.791	0.834	1.033	0.891	0.770	0.822	0.964	0.772	0.157	0.097
Er	2.32	2.44	1.91	3.12	1.98	2.26	2.31	2.82	2.52	2.21	2.28	2.85	2.30	0.38	0.25
Tm	0.337	0.354	0.279	0.455	0.285	0.324	0.338	0.405	0.373	0.316	0.329	0.438	0.354	0.048	0.035
Yb	2.19	2.31	1.74	2.81	1.82	2.11	2.12	2.50	2.37	2.01	2.09	2.93	2.35	0.30	0.22
Lu	0.334	0.350	0.270	0.420	0.269	0.318	0.316	0.371	0.355	0.299	0.315	0.463	0.375	0.047	0.032
Hf	1.55	1.67	1.46	3.03	1.52	1.75	1.77	2.56	1.66	1.67	1.43	1.80	1.25	2.54	1.32
Ta	0.23	0.24	0.24	0.83	0.45	0.39	0.37	0.51	0.33	0.39	0.21	0.06	0.10	0.14	0.07
Pb	3.04	10.22	3.67	4.47	2.91	5.51	26.48	14.46	13.44	12.76	8.38	4.83	2.13	34.86	38.68
Th	0.44	0.45	0.22	1.82	0.62	0.43	0.47	0.83	0.41	0.68	0.50	0.54	1.35	19.02	4.36
U	0.343	0.140	0.119	0.528	0.390	0.161	0.163	0.354	0.173	0.329	0.154	0.373	0.605	1.493	1.398
Ti/Y	330.94	322.97	366.35	411.32	350.01	334.42	376.46	424.09	324.80	354.57	343.79	187.60	204.22	80.26	111.01
(Sm/Yb)n	1.22	1.22	1.54	1.93	1.43	1.34	1.45	1.79	1.22	1.47	1.40	1.46	1.41	14.86	4.80

Fe_2O_3 = all Fe calculated as Fe_2O_3; LOI = loss on ignition; Mg# = $100 \times Mg^{2+}/(Mg^{2+} + Fe^{2+})$, $Fe^{3+}/Fe = 0.1$.

Table 4
Whole-rock Sm-Nd isotopic data for the Yingfeng dolerites/basalts.

Sample #	Sm (ppm)	Nd (ppm)	$^{147}Sm/^{144}Nd$	$^{143}Nd/^{144}Nd$	2σ	$\varepsilon_{Nd}(T)$
13MH-13	2.41	7.59	0.2019	0.512842	0.000017	3.4
13MH-15	4.88	19.52	0.1587	0.512480	0.000019	1.0
13MH-43	2.77	9.11	0.1926	0.512785	0.000014	3.3
13MH-44	4.02	14.03	0.1819	0.512532	0.000016	−0.5
13MH-57	2.60	7.87	0.2099	0.512904	0.000019	3.8

Notes: (1) $\varepsilon_{Nd}(T) = \{[^{143}Nd/^{144}Nd - {}^{147}Sm/^{144}Nd \times (e^{\lambda T} - 1)]/[(^{143}Nd/^{144}Nd)_{CHUR(0)} - (^{147}Sm/^{144}Nd)_{CHUR(0)} \times (e^{\lambda T} - 1)] - 1\} \times 10{,}000$, where $\lambda_{Sm} = 6.54 \times 10^{-12}$ year^{-1}; $(^{143}Nd/^{144}Nd)_{CHUR(0)} = 0.512638$; $(^{147}Sm/^{144}Nd)_{CHUR(0)} = 0.1967$.
(2) T = 850 Ma, crystallization age of the Yingfeng dolerites.

of amphibolite to high-pressure granulite facies metamorphism. The latter is coeval with the UHP eclogite-facies metamorphism (440–420 Ma) during the continental collision in North Qaidam UHPM belt (Zhang et al., 2010; Song et al., 2010, 2012, 2014; Zhang et al., 2015).

5.2. Major and minor elements

Ten samples of the Yingfeng dolerites/basalts and five samples of the Aolaoshan meta-volcanics were analyzed for major- and trace-element data (see sampling localities in Fig. 1c). The results

are listed in Table 3. They show weak alteration with low loss on ignition (LOI) of 0.3 wt.% to 2.3 wt.%. The Yingfeng dolerites/basalts have varying major element compositions with SiO_2 (44.8–52.5 wt.%, volatile-free), TiO_2 (0.9–1.8 wt.%), Al_2O_3 (12.7–17.7 wt.%), MgO (6.7–11.5 wt.%), CaO (8.4–12.6 wt.%), Fe_2O_3T (10.8–14.8 wt.%) and total alkalis ($Na_2O + K_2O$, 1.6–4.6 wt.%). Most of them show evolved compositions with low Mg number (52–60), Cr (59–263 ppm) and Ni (52–114 ppm), except for 13MH-13, 13MH-18 and 13MH-67 with high MgO (9.5–11.5 wt.%), Cr (137–600 ppm) and Mg number (63–71). They exclusively plot within the subalkaline basalt field (Fig. 6a). On the FeOT/MgO vs TiO_2 plot (Fig. 6c), the Yingfeng mafic rocks exhibit a typical tholeiitic trend. Together with the data for eclogites from Yuka, Dulan and Xitieshan in the North Qaidam UHPM belt (Fig. 6b), they can be divided into a high-Ti alkaline group [Ti/Y > 500 and $(Sm/Yb)_n$ > 2.5] and a low-Ti tholeiitic group [Ti/Y < 500 and $(Sm/Yb)_n$ < 2.5]. The Yingfeng dolerites/basalts belong to the latter group.

The Aolaoshan meta-volcanics mainly consist of basalts (Q14-85/87/89) and rhyolites (Q14-83/84). Sample Q14-85 plots within the subalkaline basalt field, while Q14-87/89 belong to the andesite/basalt field (Fig. 6a). Q14-85 has a less evolved composition with low SiO_2 (43.5 wt.%), Na_2O (2.8 wt.%), and K_2O (0.4 wt.%), but high MgO (9.6 wt.%), TiO_2 (1.3 wt.%), Cr (305 ppm), and Ni (146 ppm) compared to Q14-87/89. There is a calc-alkaline trend from Q14-85 to Q14-87/89 (Fig. 6c). Two Aolaoshan felsic rocks (Q14-83/84) are generally high in SiO_2 (70.4–72.1 wt.%) and K_2O (7.6–8.8 wt.%), but low in Na_2O (~2.3 wt.%), MgO (0.1–0.2 wt.%), Fe_2O_3T (0.4–0.5 wt.%), CaO (1.9–2.0 wt.%), and TiO_2 (~0.1 wt.%). They are metaluminous with A/CNK (0.96–0.97) and A/NK (1.20–1.27) values, and plot in the rhyolite to dacite fields (Fig. 6a).

On the chondrite-normalized REE diagrams (Sun and McDonough, 1989; Fig. 7f and 7 h), the Yingfeng and Aolaoshan mafic rocks show uniform and moderate LREE enrichments (La_N/Yb_N = 1.2–3.8), weak HREE depletions (Gd_N/Yb_N = 1.1–1.6) and slight Eu anomalies ($\delta Eu = Eu_N/\sqrt{Sm_N \times Gd_N}$ = 0.86–1.15). Similarly, the low-Ti eclogites from Yuka, Xitieshan and Dulan exhibit intermediate enrichments in LREE (mostly La_N/Yb_N = 1.2–5.9) and insignificant Eu anomalies (mostly δEu = 0.84–1.14), while the high-Ti group of Yuka eclogites shows relatively strong HREE fractionation (dominantly Gd_N/Yb_N = 1.6–3.2) which may indicate the presence of garnet as a residual phase in the mantle source region (Fig. 7b and d).

On the primitive mantle-normalized spider diagram (Sun and McDonough, 1989; Fig. 7e), the Yingfeng dolerites/basalts have smooth patterns characterized by insignificant negative anomalies of high field strength elements (HFSE) with Nb/La (0.9–1.2) and Nb/Th (8.2–14.9) slightly lower than those of E-MORB (Nb/La = 1.3, Nb/Th = 13.8; Sun and McDonough, 1989), but similar to those of Deccan low-Ti basalts (Melluso et al., 2006). In contrast, the Aolaoshan basalts show variable depletion in Nb, Ta, Zr, Hf and Ti relative to the neighboring elements (Nb/La = 0.1–0.8 and Nb/Th = 0.9–6.0; Fig. 7g). On the whole, the low-Ti eclogites (Yuka, Dulan and Xitieshan) show increasing enrichments from Lu to Th with weak to negative anomalies in Nb-Ta (mainly Nb/La = 0.4–1.6 and Nb/Th = 2.6–15.7; Fig. 7a and c). However, the uniform "humped" patterns characterized by the positive anomalies of HFSE (Nb/La = 1.3 ± 0.2 and Nb/Th = 14.8 ± 2.6, n = 17) for the Yuka high-Ti group are similar to that of modern oceanic island basalt (Nb/La = 1.3 and Nb/Th = 12; Sun and McDonough, 1989) and the Suxiong alkaline basalts in South China (Li et al., 2002; Fig. 7a).

The Aolaoshan felsic rocks are characterized by strong LREE-enrichment (La_N/Gd_N = 13.1 and 8.2) and HREE-depletion (Gd_N/Yb_N = 7.2 and 3.0), and no Eu anomalies to significant positive anomalies (δEu = 0.93 and 2.33), which may be attributed to residual garnet and plagioclase accumulation, respectively (Fig. 7h). The multi-element diagram shows pronounced troughs in Nb-Ta-Ti and peaks in Th-U relative to neighboring elements (Fig. 7g).

5.3. Sm-Nd isotopes

Five samples of the Yingfeng dolerites/basalts were analyzed for Sm-Nd isotopes. The results are presented in Table 4. They have consistent $^{147}Sm/^{144}Nd$ ratios (0.16–0.21) and moderate $^{144}Nd/^{143}Nd$ ratios (0.512480–0.512904) with initial εNd(T) values (−0.5 ~ +3.8), indicating that they were derived from a time-integrated depleted mantle. All the initial values of Nd isotope for the North Qaidam eclogites were also recalculated at 850 Ma. The high-Ti group of the Yuka eclogites exhibits high and positive εNd(T) values (+4.2 to +5.1). However, the low-Ti eclogites from Xitieshan and Yuka commonly have a wide range of initial Nd isotope compositions [εNd(T) = +1.2 ~ + 5.9], which are similar to those of Yingfeng dolerites/basalts, but significantly distinct from the initial Nd isotopic value of contemporaneous depleted mantle [εNd(850 Ma) = +8.1].

6. Petrogenesis

6.1. Effect of alteration on magma compositions

Although the Yingfeng dolerites/basalts and Aolaoshan meta-volcanics have low LOI (0.3–2.3 wt.%), the mobility of major and trace elements still need to be evaluated prior to the discussion on petrogenesis, especially when comparisons are made with the Yuka, Dulan and Xitieshan eclogites. The effects of alteration and metamorphism on major element contents can be monitored by the CIA value [$Al_2O_3/(Al_2O_3 + CaO + Na_2O + K_2O)$ in molecular

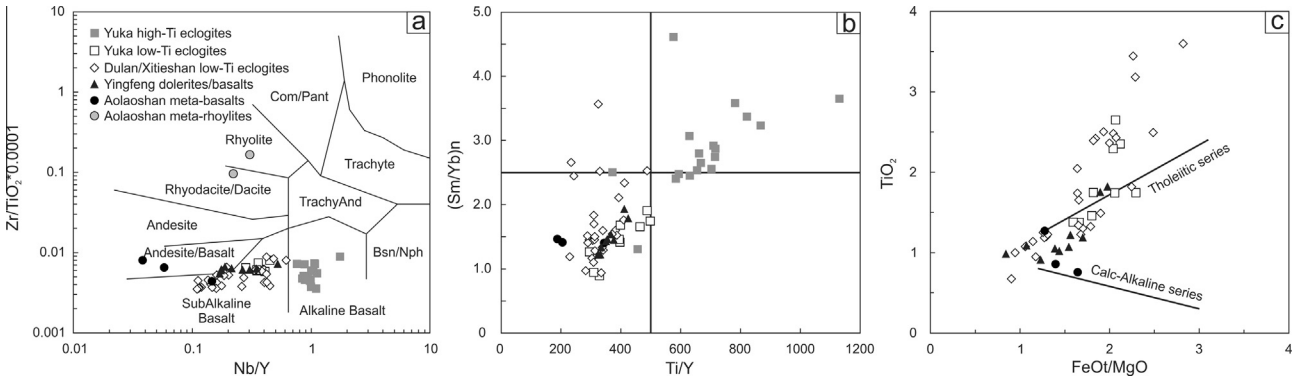

Fig. 6. (a) Nb/Y versus $Zr/TiO_2 \times 0.0001$ diagram (Winchester and Floyd, 1976). (b) Ti/Y versus $(Sm/Yb)_n$ (subscript n denotes "chondrite-normalized"). (c) FeOt/MgO versus TiO_2 diagram (Miyashiro, 1974).

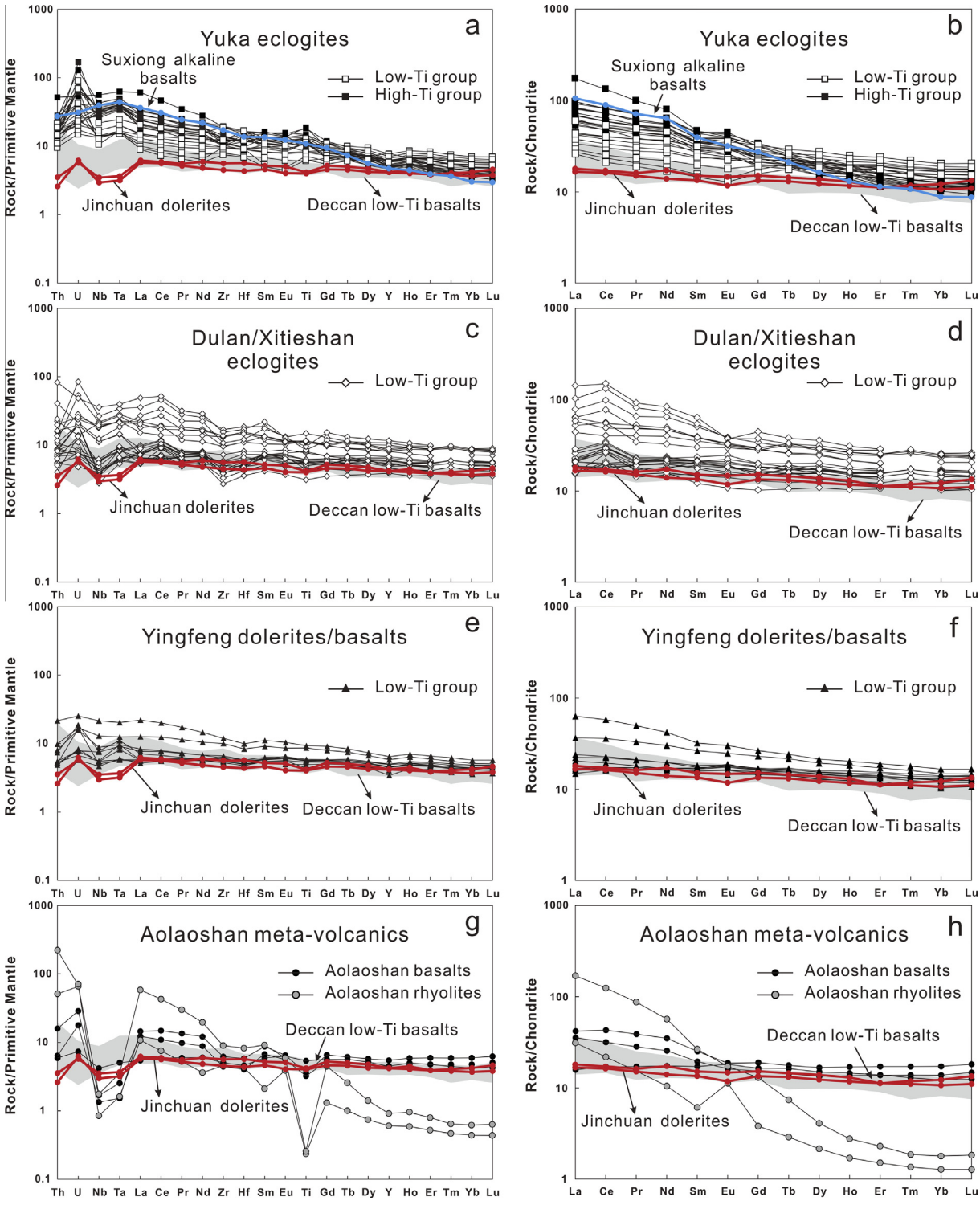

Fig. 7. Primitive mantle-normalized incompatible trace element spidergrams and chondrite-normalized REE diagrams for the North Qaidam eclogites, Yingfeng dolerites/basalts and Aolaoshan meta-volcanic rocks. Data for the Yuka eclogites are from Chen et al. (2009b) and Song et al. (2010); the Dulan and Xitieshan eclogites from Zhang et al. (2012) and Yu et al. (2013). The average value of Suxiong alkaline basalts (blue line) in the Kangdian Rift of South China is from Li et al. (2002). The values for Jinchuan dolerites (red lines) are from Li et al. (2005). The low-Ti basalts data for the Deccan LIP (grey domain) are from Melluso et al. (2006). The normalization values are from Sun and McDonough (1989). (For interpretation of the references to color in this figure legend, the reader is referred to the web version of this article.)

proportions; Nesbitt and Young, 1982]. The CIA values of the Yingfeng–Aolaoshan mafic rocks are in a limited range of 34–47%, consistent with those of fresh basalts (CIA = 30–45%; Nesbitt and Young, 1982). The North Qaidam eclogites have relatively variable but similar CIA values (29–49) to those of fresh basalts. The CIA values (~49) of the Aolaoshan felsic rocks also fall within the interval of fresh granitic rocks (CIA = 45–55, Nesbitt and Young, 1982). These recognitions can be also supported by the A-CN-K and A-CNK-FM triangular diagrams (Appendix Fig. 1, Nesbitt and Young, 1989).

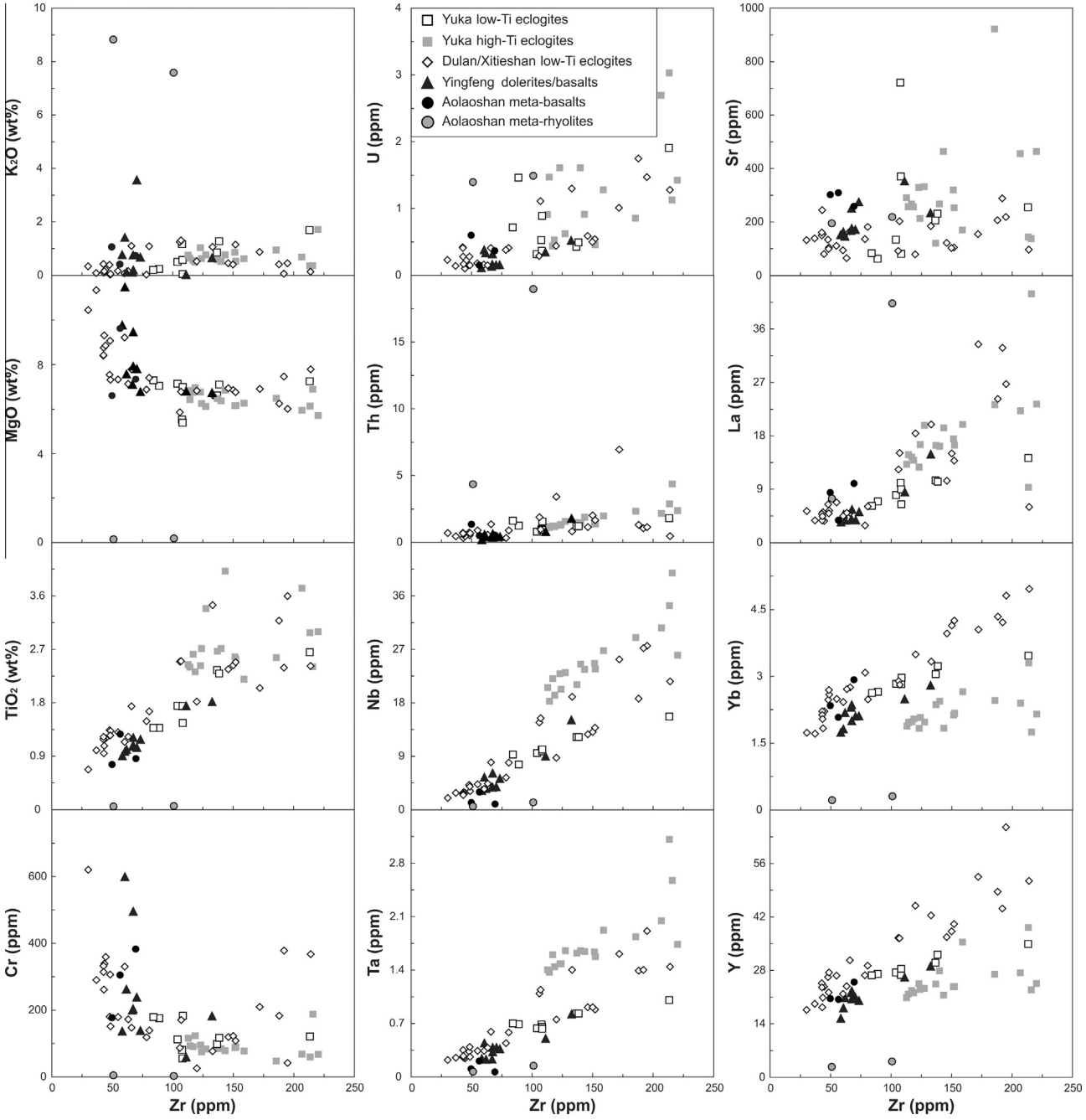

Fig. 8. Correlation diagrams of zirconium versus selected major and trace elements to evaluate their possible mobilities.

The mobility of trace elements can be assessed by plotting against Zr or CIA values (Li et al., 2008b, 2010b). In the covariance diagrams (Fig. 8), the rare earth elements (REE, such as La and Yb), Y, HFSE (Th, Zr, Hf, Nb, Ta, Ti) and compatible elements (Cr and Ni) show linear relationships with Zr, which indicate they are immobile during later alteration and metamorphism, although the alkaline high-Ti and tholeiitic low-Ti groups show distinct trends. Therefore, we will only use the immobile elements in the following discussion.

6.2. Fractional crystallization

Most of the mafic rocks in North Qaidam show the characteristics of evolved magmas in disequilibrium with primary melts which have Mg# > 72, Cr > 1000 ppm and Ni > 400 ppm (Wilson, 1989; Niu and O'Hara, 2008). Sample 13MH-18 from the Yingfeng dolerites/basalts is least-evolved with high MgO (11.5 wt.%), Mg# (71), and compatible element contents (Cr = 600 ppm and Ni = 178 ppm), and is closest to the composition of picritic magma (MgO = 12 wt.%; Le Bas, 2000). For the Yingfeng–Aolaoshan mafic rocks, the positive correlation between Mg# and compatible elements (Cr and Ni) indicate the fractional crystallization dominantly of olivine and clinopyroxene in magma chambers or en route to the surface (Fig. 9d and f). The linear relationship between CaO/Al_2O_3 and Mg# may be also ascribed to the fractionation of clinopyroxene (Fig. 9b). The slight Eu anomalies (δEu = 0.86–1.15) suggest that plagioclase may not be a major fractionating phase. The Fe-Ti oxides might not have preferentially crystallized in view of

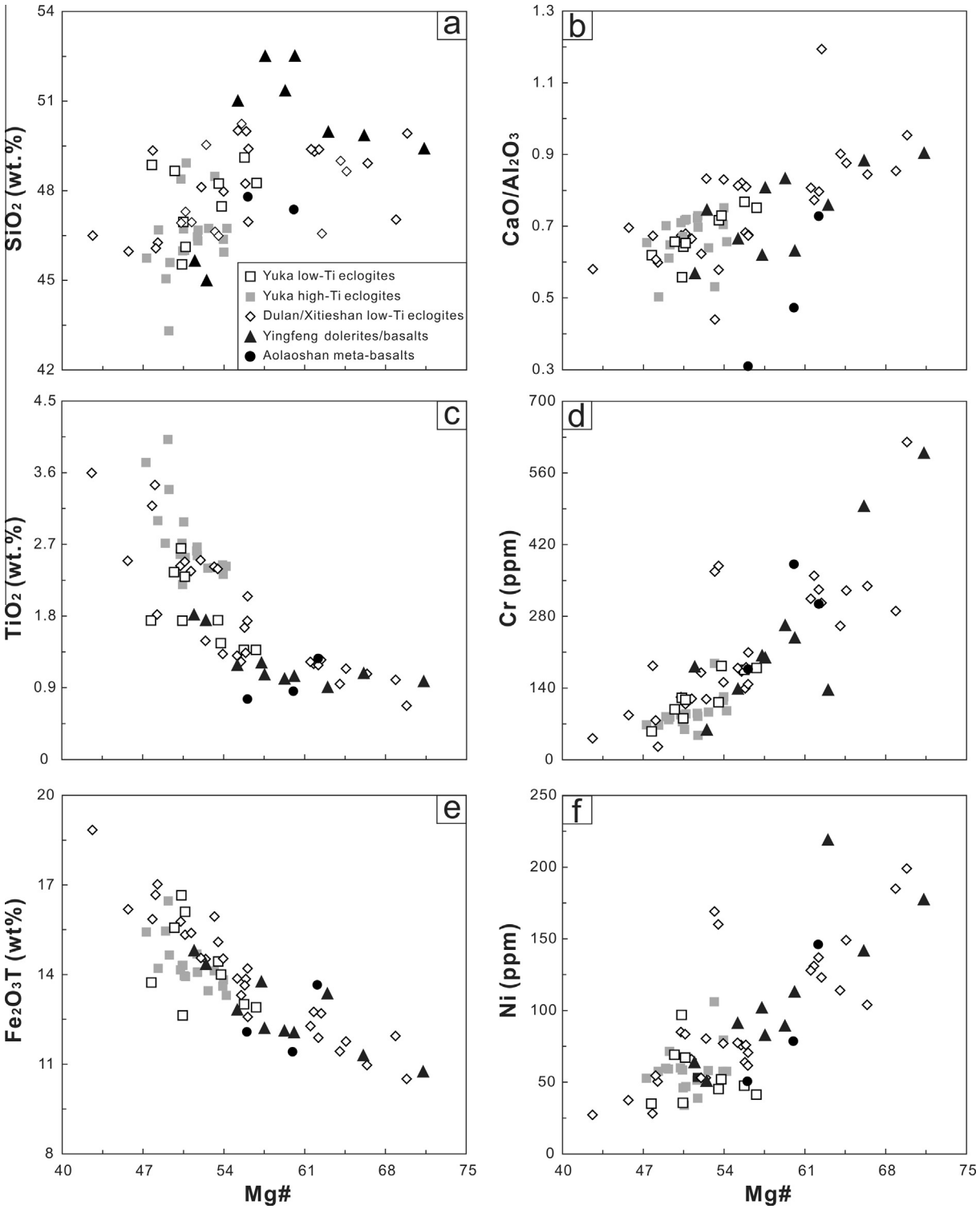

Fig. 9. Mg-number variation diagrams for mafic rocks in the North Qaidam UHPM belt.

the weak to absent Ti anomalies and the tholeiitic trend, except for Q14-87 and Q14-89 (Fig. 9c and e). Similarly, for the North Qaidam eclogites, the negative correlation (Mg# vs. TiO_2) and positive correlation (Mg# vs. Ni) are consistent with significant crystal fractionation of olivine (Fig. 9c and f), whereas plagioclase is unlikely to be an important fractionating phase on account of the lack of Eu anomalies (Fig. 7).

6.3. Lithospheric contamination and source

The involvement of continental crust and enriched lithospheric mantle would significantly change the LREE/HFSE and HFSE/LILE ratios in primitive parental magmas (Hofmann, 1988). Among the mafic rocks in North Qaidam, the high-Ti eclogites in Yuka show positive HFSE anomalies [$(La/Ta)_{PM}$ = 0.51–0.97; $Ti^* = 2Ti_{PM}/$

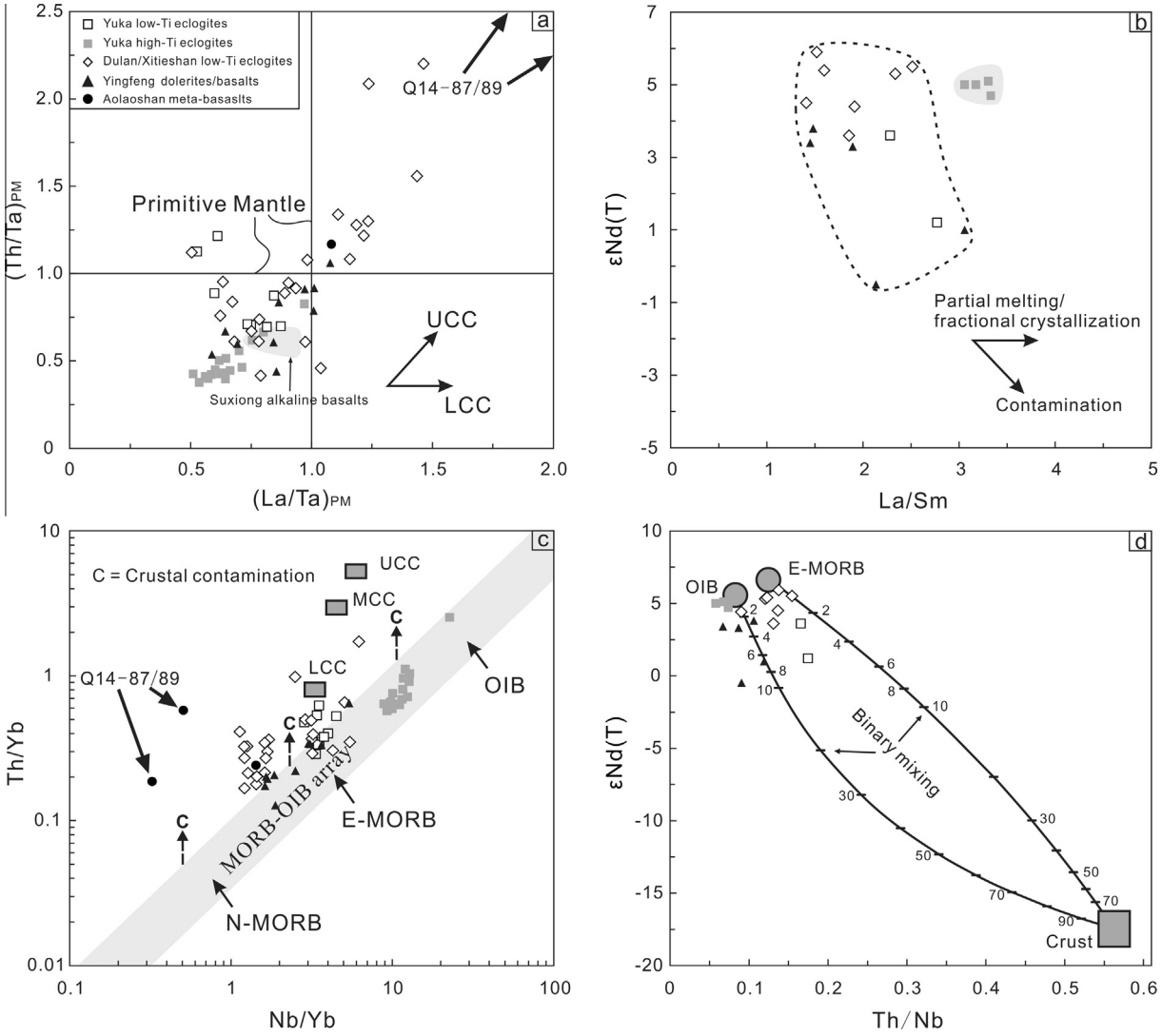

Fig. 10. Plots of (a) $(Th/Ta)_{PM}$ vs. $(La/Ta)_{PM}$ (Ingle et al., 2002), UCC-upper continental crust, LCC-lower continental crust, the normalization values of primitive mantle are from Sun and McDonough (1989), the Suxiong alkaline basalts are from Li et al. (2002). (b) εNd(T) vs. La/Sm. (c) Th/Yb vs. Nb/Yb (Pearce, 2008), the values of the upper, middle and lower continental crust are from Rudnick and Gao (2003). (d) εNd(T) vs. Th/Nb, the numbers labeled on the binary mixing curve represent the percentages of crust material added to mantle melt. The contaminant crustal component [Th = 18.6 ppm, Nb = 33.1 ppm, Nd = 105.3 ppm, εNd(850 Ma) = −17.5] is the representative Mesoproterozoic Yingfeng rapakivi granite (Qy76 from Hu et al. (2007)). The composition of OIB [Th = 2.4 ppm, Nb = 28.6 ppm, Nd = 30.3 ppm, εNd(850 Ma) = +5.6] is the average of least-contaminated alkaline basalts in the Suxiong volcanic rocks (99KD22-4, 99KD22-5, 99KD22-8 from Li et al. (2002)). The composition of E-MORB [Th = 0.6 ppm, Nb = 4.4 ppm, Nd = 20.2 ppm, εNd(850 Ma) = +6.7] is the average of least-contaminated Shangshu basalts in northern Zhejiang (except for 99SC75 from Li et al. (2008b)).

$(Sm_{PM} + Tb_{PM}) = 0.82–1.76$; subscript PM denotes primary mantle-normalized], which imply negligible contamination of crust or enriched SCLM (Fig. 10a and c). This conclusion is also supported by positive and uniform initial εNd values (4.7–5.1; see Fig. 10b and d). However, the low-Ti eclogites in Yuka, Dulan and Xitieshan show relatively varying anomalies in Nb-Ta and diverse initial Nd isotopic values (Fig. 10a–c), which imply that the crustal contamination plays a role in magma differentiation, although some are not appreciably contaminated. They are similar to the Jinchuan dolerites, which were recognized to involve lithosphere interaction (Li et al., 2005; Fig. 7). The linear relationship of $(La/Ta)_n$ vs. $(Th/Ta)_n$ indicates the mixing between mantle melts and upper continental crust (Fig. 10a; Ingle et al., 2002). The quantitative modeling suggests that they may origin from E-MORB source and have experienced a minor crustal assimilation (<4%; Fig. 10d).

The Yingfeng dolerites/basalts and one Aolaoshan basalt (Q14-85) exhibit weak enrichments in Nb-Ta [$(La/Ta)_{PM} = 0.59–1.08$] and dominantly positive εNd(T) values (1.0–3.8), which are similar to those of the least-contaminated low-Ti eclogites (Fig. 10a and b). These characteristics imply that these mafic rocks suffered little, if any, crustal assimilation. Minor assimilation (<8%) may exist given the weak correlation of Th/Ta with εNd(T) values (Fig. 10d). It is noted that the Yingfeng dolerites/basalts perhaps experienced heterogeneous source mixing (e.g. mantle plume and depleted asthenosphere mantle) and/or magma mixing (e.g. OIB and E-MORB/N-MORB), in consideration of their relatively high Th/Nb but low La/Sm compared to the high-Ti group (Fig. 10b and d). On the contrary, samples Q14-87 and Q14-89 of the Aolaoshan basalts are characterized by significant negative HFSE anomalies (Fig. 10a and c), and have lower Nb/La ratios (0.10–0.14) than that of the upper continental crust (Nb/La = 0.39; Rudnick and Gao, 2003), implying that the Nb-Ta anomalies could not have derived from crustal contamination. Furthermore, the assimilation of crustal materials is unable to cause the obvious negative anomalies in

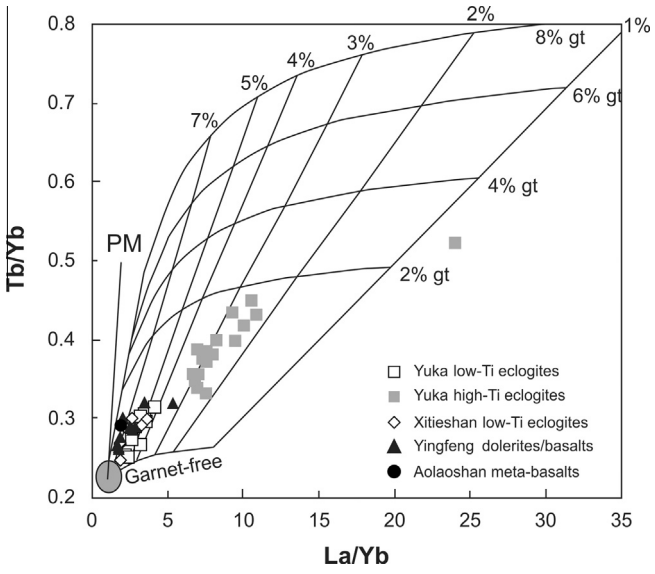

Fig. 11. Plot of La/Yb vs. Tb/Yb for the Yingfeng–Aolaoshan dolerites/basalts and North Qaidam eclogites. The melting curves are from George and Rogers (2002). The ratios of primitive mantle (PM) are from Sun and McDonough (1989). The contaminated low-Ti eclogites and Aolaoshan meta-basalts (Q14-87/89) have been excluded. One high-Ti sample plots outside of the fractional melting grid, perhaps due to a distinct mantle source or lower degree of melting.

Zr-Hf of samples Q14-87/89. Thus we suggest that their depletions in HFSE are most likely inherited from a metasomatized subcontinental lithosphere mantle (SCLM).

It is noteworthy that the low-Ti and high-Ti groups exhibit obviously different Ti/Y and $(Sm/Yb)_n$ ratios (Fig. 6b). In fact, the fractionation of REE may be ascribed to the AFC processes or to the partial melting, including the effects of residual minerals, melting degree and source heterogeneity. On the plot of La/Yb vs. Tb/Yb (Fig. 11), the high-Ti basalts might be generated by the low degree (2–4%) partial melting of a deep garnet-bearing (0–2%) asthenospheric mantle source. However, the higher degree (>4%) of melting occurred in a residual spinel-stable field for the low-Ti group.

For the Aolaoshan rhyolites (Q14-83/84), the distinct evolved trends in most Zr versus major and minor elements plots (Fig. 8) suggest that they may not have formed by AFC processes of the coeval Aolaoshan basaltic magma. The partial melting of mafic rocks can hardly produce the abnormal low Na_2O/K_2O ratios (0.26–0.30), MgO contents (0.1–0.2 wt.%) and compatible element concentrations (Cr = 2.5–4.1 ppm and Ni = 2.3–2.4 ppm). The strong REE fractionation and high Sr/Y ratios (52.7–70.9) imply a source with residual garnet (Fig. 7h). However, the residual phases were most likely dominated by plagioclase, because of the low Sr concentrations (195–219 ppm). The Aolaoshan rhyolites are characterized by high K_2O/Na_2O (3.3–3.8), CaO/Na_2O (0.8–0.9) and low Rb/Ba (0.25–0.65), Rb/Sr (0.82–1.11), indicating a potassic, clay-poor greywacke source (Sylvester, 1998). Similarly, the ca. 800 Ma S-type granitoids from the Qilian and South China blocks are characterized by high CaO/Na_2O (>0.3), low Rb/Sr (0.48–2.7), low Rb/Ba (0.1–0.7) and negative barium anomalies, and are derived from clay-poor psammitic rocks (Tung et al., 2013 and references herein).

6.4. Tectonic setting

Despite experiencing variable extents of fractional crystallization and involvement of crustal contamination, the high-Ti eclogites from Yuka show OIB-like Nd isotopic compositions and trace element patterns which are comparable with those of the Suxiong alkali basalts (Li et al., 2002; Fig. 7a–b), while the least-contaminated samples of low-Ti group exhibit E-MORB patterns which are similar to those of the Deccan low-Ti basalts (Fig. 7e–h). Among the Yingfeng dolerites/basalts, samples 13MH-13/18/67 are least-evolved, and have the highest MgO contents (9.5–11.5 wt.%) and compatible elements. With these samples, we calculated the compositions of primary magma based on the procedure of Herzberg et al. (2007) and Wang et al. (2009), which are picritic melts and contain 48.4–49.2 wt.% SiO_2, 1.0–1.1 wt.% Fe_2O_3, 8.9–11.2 wt.% FeO and 14.0–17.7 wt.% MgO. In terms of the equation T_p (°C) = 1463 + 12.74MgO − 2924/MgO (Herzberg and O'Hara, 2002), the potential temperatures (1434–1524 °C) are obtained, which are higher than that of contemporary ambient MORB-source asthenosphere mantle (1350–1450 °C; references in Li et al., 2008b), implying an origin of anomalously hot mantle source. In addition, the North Qaidam mafic rocks are characterized by high Ti/V, mostly >20 for the low-Ti tholeiitic group and >50 for the high-Ti alkaline group, compatible with continental flood tholeiites and ocean-island basalts, respectively (Fig. 12a; Shervais, 1982). In the discrimination diagrams of Y/15-La/10-Nb/8 (Fig. 12b) and Hf/3-Th-Ta (Fig. 12c), the high-Ti eclogites from Yuka are plotted in the within-plate basalt field. However, most mafic rocks of the low-Ti group belong to E-MORB and continental basalts. In contrast, some Dulan/Xitieshan low-Ti eclogites and two of the Aolaoshan basalts (Q14-87/89) are similar to continental back-arc tholeiites and island arc basalts, which might be ascribed to relatively high degree melting (and/or spinel-stable source) and crust/source contamination (see discussion above). Overall, the low-Ti and high-Ti mafic rocks in North Qaidam are likely to form in an intraplate environment related to mantle plume activities, like Emeishan, Siberian, Deccan and other LIPs in the world (Sharma et al., 1992; Hawkesworth et al., 1995; Xu et al., 2001; Melluso et al., 2006; Jowitt and Ernst, 2013; Ernst, 2014).

7. Discussion

7.1. Protoliths of North Qaidam UHPM eclogites: CFBs subducted to depths of ~120 km

Mafic rocks including basalts and associated intrusions can provide the materials for HP/UHP metamorphism during the subduction of oceanic or continental lithosphere. In the last decade, the origin and age of eclogite protoliths in North Qaidam UHPM belt have been studied (Song et al., 2014 and references therein). The eclogite blocks are dominantly derived from the 850–820 Ma CFBs with minor fragments of the 540–500 Ma oceanic crust (e.g., Zhang et al., 2008, 2010; Chen et al., 2009b; Song et al., 2009, 2010; Yu et al., 2013).

Eclogites with protoliths of 850–820 Ma CFBs in the North Qaidam UHPM belt have similar occurrences to the Yingfeng dolerites/basalts and Aolaoshan meta-volcanic rocks (Figs. 2 and 4). Their geochemical characteristics and protolith ages demonstrate that the Yingfeng dolerites/basalts and Aolaoshan layered volcanic rocks could act as the protoliths of the eclogites in the 400-km-long North Qaidam UHPM belt. The Yingfeng greenschist-facies dolerite dikes and layered basalts are indeed remnants of unsubducted CFBs on the continental margin (less than 20 km in depths). The Aolaoshan volcanic sequence, on the other hand, had undergone amphibolite facies to HP granulite facies metamorphism (40–60 km) at ~439 Ma, while most of mafic rocks in the northern margin of the Qaidam Basin were subducted to upper mantle depths (~120 km) and experienced the ultra-high pressure metamorphism (Fig. 13).

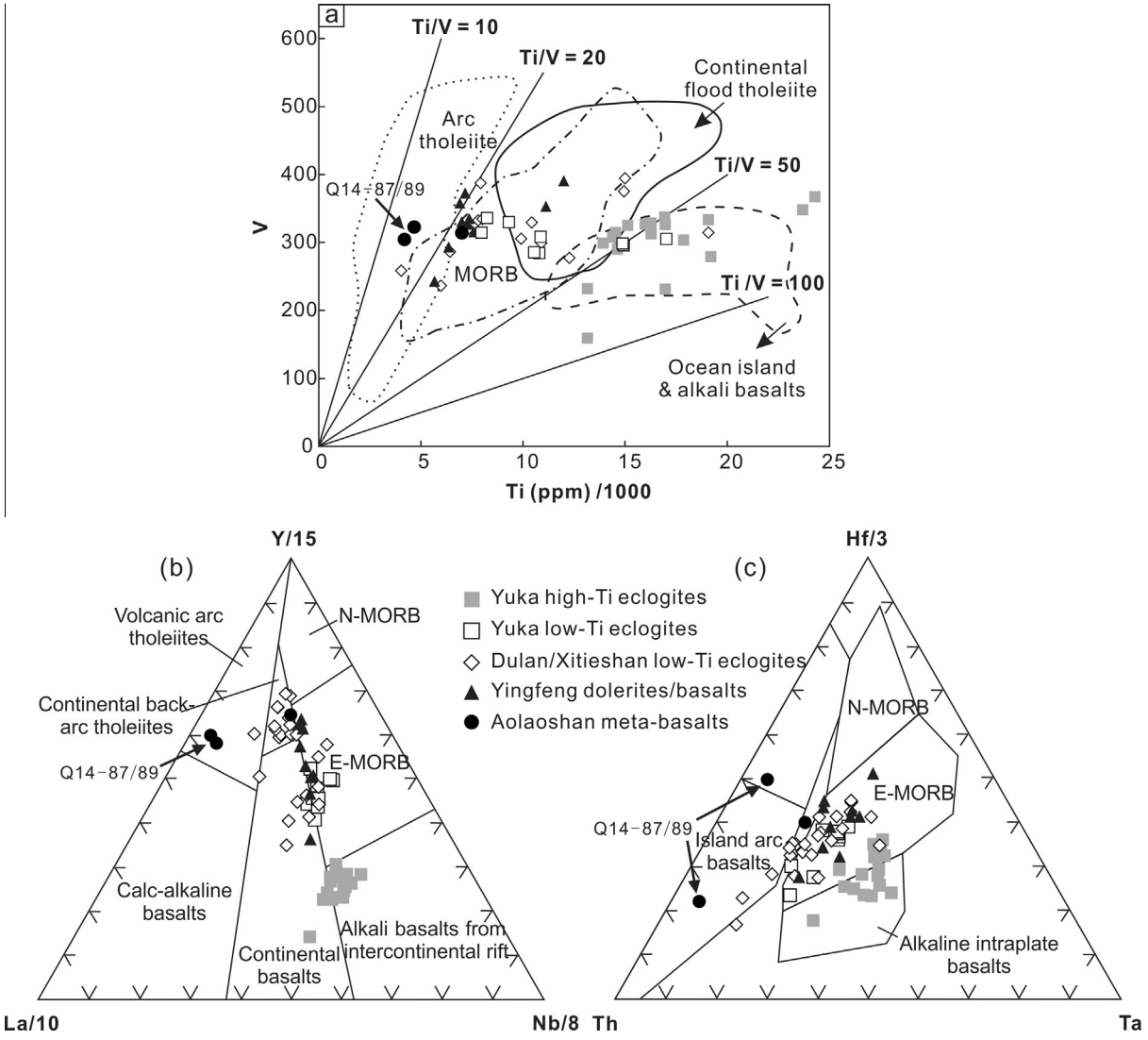

Fig. 12. Discrimination diagrams of (a) Ti vs. V (Shervais, 1982). (b) La-Y-Nb (Cabanis and Lecolle, 1989). (c) Th-Hf-Ta (Wood, 1980).

7.2. Determination of the 850–820 Ma North Qaidam LIP along the dismembered continental margin of Rodinia

Because of the dismemberment during continental breakup and strong erosion/cover/metamorphism afterwards, the 850–820 Ma mafic–ultramafic igneous rocks are dispersedly preserved in the neighboring blocks, such as Tarim, South China and Australia (Fig. 1a).

In the Longshoushan terrane of the Alxa (Alashan) block (Site 3 in Fig. 1a), the Jinchuan ultramafic–mafic intrusion, which contains the world second-large Cu–Ni sulfide ore, was dated at ~828 Ma (Li et al., 2005 and references therein). Integrated mineralogical, petrological and geochemical data are consistent with a mantle plume origin (Li et al., 2005). In addition, the Kuluketage dolerite dike swarms crop out in the northeastern margin of Tarim, and zircon U-Pb SHRIMP analyses yield a similar Neoproterozoic age of 824 ± 9 Ma (Site 4 in Fig. 1a; Zhang et al., 2009). In northwestern Yangtze, the Bikou basalts are mainly tholeiitic in composition and erupted at 821 ~ 811 Ma (Site 2 in Fig. 1a). They are likely the remnants of CFBs derived from a ~825 Ma mantle plume with recycled components and an anomalously hot asthenosphere source −150 °C hotter than the contemporary ambient MORB source (Wang et al., 2008). In the Kangdian rift of western Sichuan, the V-Ti and Cu–Ni bearing Gaojiacun mafic–ultramafic layered intrusions together with the coeval granitoids were formed in an extensional continental rift at 825 ± 12 Ma (Site 1 in Fig. 1a; Zhu et al., 2006). In northern Guangxi, the 825 Ma mafic–ultramafic dikes and sills are identical in age to the 827 Ma Gairdner-Amata dike swarm of central and southeast Australia, thought to be of mantle plume origin (Site 9 in Fig. 1a; Wingate et al., 1998; Li et al., 1999). The intraplate geochemical signatures (E-MORB or OIB) and high mantle potential temperatures (>1480 °C) imply the presence of a Neoproterozoic mantle plume beneath South China (Wang et al., 2009 and references herein). These simultaneous magmatic rocks in South China were termed the Guibei LIP by Ernst et al. (2008). Recently, a large amount of plume-related igneous activities during this period have also been recognized in the eastern segment of the Nanhua rift basin (Site 10 in Fig. 1a), for example the 849 Ma Zhenzhushan bimodal volcanic rocks, the 836–857 Ma Wuyi basalts/gabbros, the 848 Ma Gangbian alkaline complex and the 849 Ma Shenwu dolerite dikes (Li et al., 2008b, 2010a,b; Shu et al., 2011).

The synchronous igneous rocks in North Qaidam extend more than 400 km from the Dulan UHPM terrane in the east to Yingfeng–Aolaoshan region in the west (Fig. 1b). As discussed above, parts of them had been subducted to depths more than 120 km

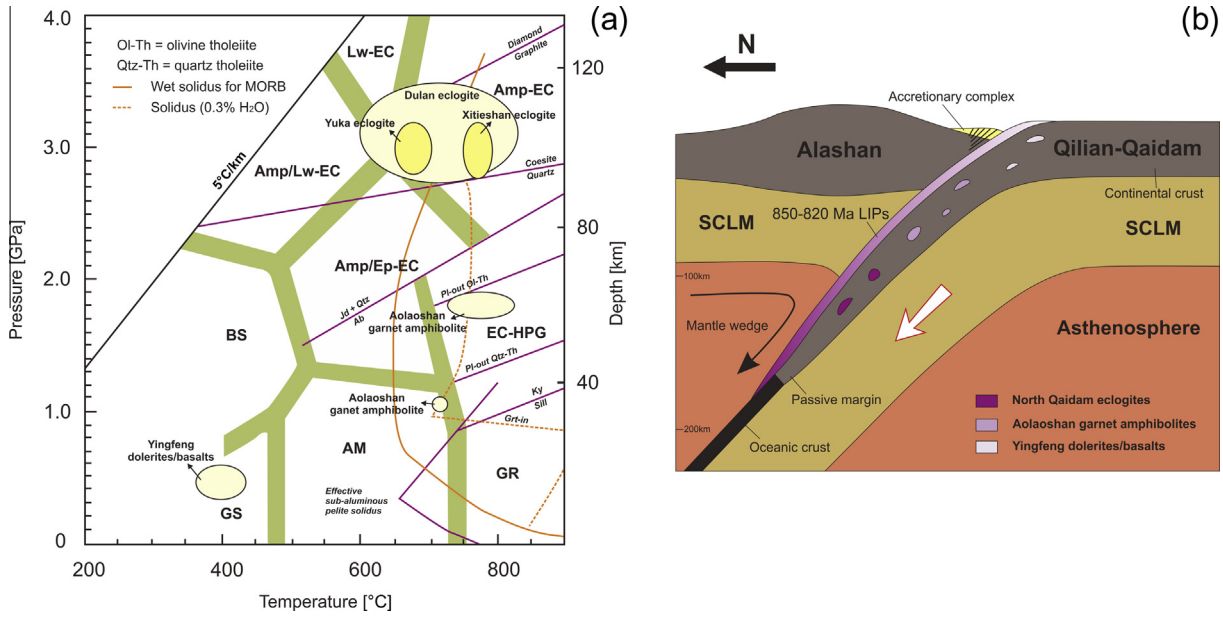

Fig. 13. (a) The peak metamorphic *P–T* conditions of North Qaidam eclogites, Aolaoshan garnet amphibolites, and Yingfeng dolerites/basalts. *P–T* boundaries of various metamorphic facies [greenschist (GS), amphibolite (AM), granulite (GR), medium temperature eclogite-high pressure granulite (EC-HPG), blueschist (BS), amphibole-epidote eclogite (Amp/Ep-EC), amphibole lawsonite eclogite (Amp/Lw-EC), lawsonite eclogite (Lw-EC), and amphibole eclogite (Amp-EC)] are according to Brown (2009). (b) The speculative distribution of the 850–820 Ma LIP along the subducted continental margin of the Qilian-Qaidam block. (For interpretation of the references to color in this figure legend, the reader is referred to the web version of this article.)

(e.g., Yuka, Xitieshan and Dulan eclogites), some were metamorphosed at middle-lower crust level (e.g., the Aolaoshan amphibolites), and others remained at surface or shallow crustal levels with greenschist-facies metamorphism at most (e.g., the Yingfeng dolerites/basalts), as illustrated in Fig. 13b. By using the simple "lithosphere bending model" and assuming 350 km bending radius of continental lithosphere like Himalaya (Leech et al., 2005), the arc length and radian from shallow to deep locations can reach to 270 km and 0.775, respectively. The subducted LIP component would occupy an area of 270 × 400 km^2 on the rifted passive continental margin of the Qaidam block. Consequently, we speculate that the 850–820 Ma North Qaidam LIP must have an areal extent of >100,000 km^2, the minimum dimension criterion considered for the standard LIPs (Coffin and Eldholm, 1994; Bryan and Ernst, 2008; Ernst, 2014), provided that the concurrent magmatic records in the adjacent blocks are also taken into account.

The dismembered 850–820 Ma LIP records in Tarim, South China, Qilian–Qaidam and even Australia, like other well-known reconstructed LIPs in the world (e.g., Paraná–Etendeka, North Atlantic Igneous Province, Deccan, Karoo, etc), may provide strong evidence for that these blocks have close affinities before being separated. Actually, the Grenville-age orogenic belt extends from the Yangtze block in the east, via Qaidam–Qilian in the middle, and to Tarim in the west, in favor of the proposal of the "South-West China United Continent" (Song et al., 2012; Fig. 1a). In addition, the latest Neoproterozoic continental rift basalts (~600 Ma) in the North Qilian Orogen and central-southeastern Australia also support a link of the Qilian–Qaidam block between SE Australia and South China during the final breakup of Rodinia (Xu et al., 2015). The abundance and planar distribution of coeval (850–820 Ma) igneous rock associations from deep to shallow and on the surface, including mafic to ultramafic sills and intrusions (Jinchuan, Gaojiacun), dikes and flood basalts (Yingfeng, Bikou, Kuluketage, Gairdner-Amata), are consistent with the features of LIPs induced by a superplume (Ernst et al., 2005, 2008).

7.3. Tectonic evolution from supercontinental breakup to continental collision and subduction

In general, the formation and evolution of most LIPs are temporally and spatially associated with continental breakup and opening of oceanic basins, although the Siberian and Emeishan LIPs seem to correlate with aborted rifting (Richards et al., 1989; White and McKenzie, 1989; Coffin and Eldholm, 1994; Courtillot et al., 1999; Saunders, 2005; Ernst et al., 2005). Fig. 14 illustrates the dynamic evolution process from an ascending mantle superplume and the formation of LIP (pre-rift phase; Fig. 14a), subsequently to the formation of rift basin and passive margin (syn-rift phase; Fig. 14b), and then to the seafloor spreading (Fig. 14c) and the final subduction of oceanic–continental lithosphere (Fig. 14d-e).

(a) An ascending mantle plume which arrived at the base of lithosphere could melt by adiabatic decompression/high potential temperature and cause the lithosphere (metasomatized SCLM and lower crust) to melt by conductive heating, which rapidly produced a large amount of igneous rocks (flood basalts, mafic dikes/sills, layered mafic–ultramafic intrusions, anorogenic granitoids) to form the 850–820 Ma LIP. Like most continental LIPs (Afro-Arabian, North Atlantic Igneous Province, Deccan, Paraná, Karoo and Central Atlantic Magmatic Province), the pre-rift magmatism also occurred at Tarim, South China, Qilian–Qaidam and SE Australia during the breakup of Rodinia (Fig. 14a). The North Qaidam LIP mainly consists of the 844–821 Ma Yingfeng–Aolaoshan dolerite dikes and flood basalts, the 850–820 Ma CFB protolith of the North Qaidam eclogites, and the 828 Ma Jinchuan ultramafic intrusions-dolerite dikes. It represents a dismembered LIP (originally >100,000 km^2 in area) along the passive continental margin. Other contemporaneous plume-related magmatic records in South China, Tarim and

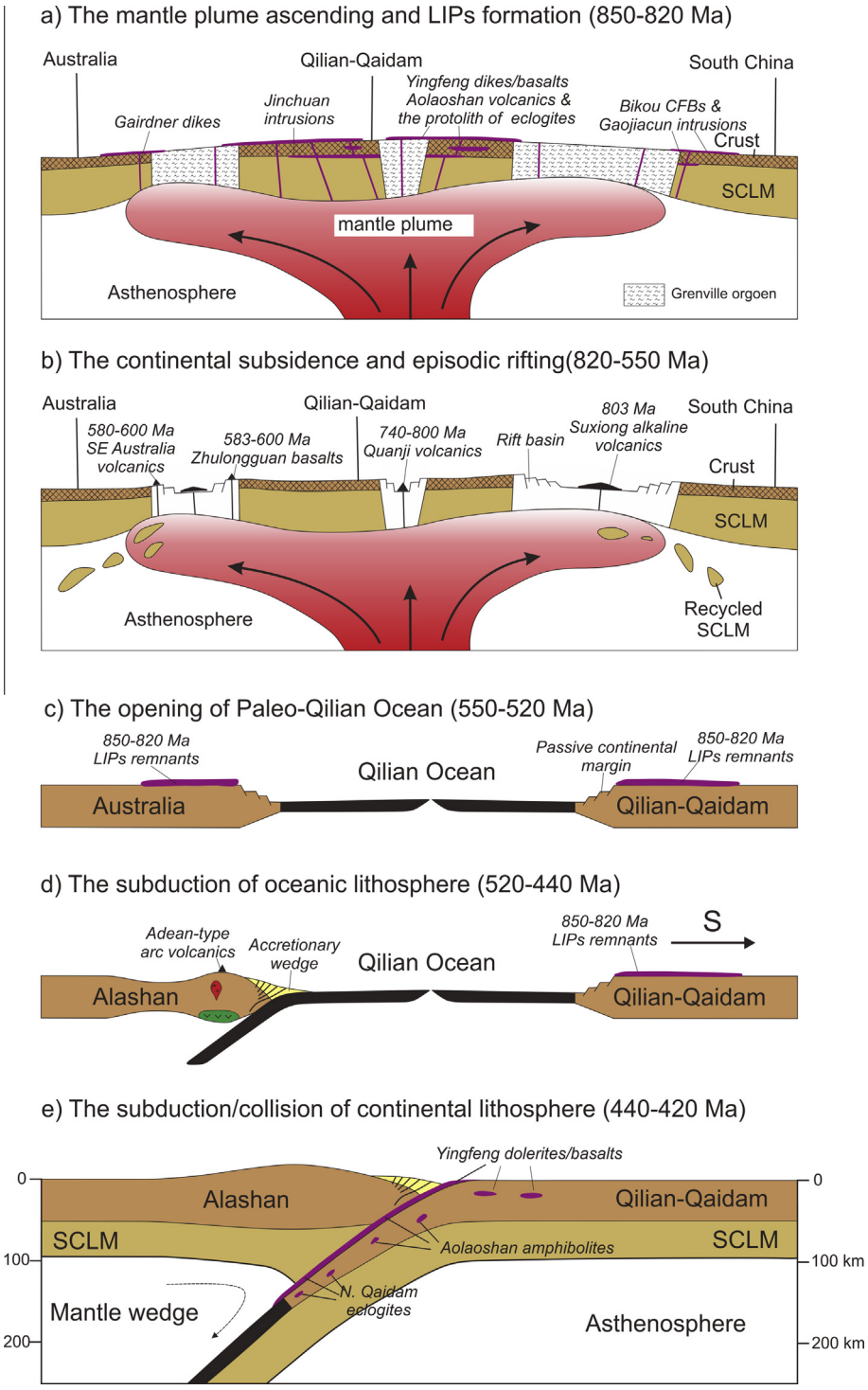

Fig. 14. Tectonic model showing a complete evolution from supercontinent breakup in the Neoproterozoic, to sea-floor spreading, oceanic and continental subduction/collision in the Early Paleozoic.

Australia include the 825 Ma Gairdner dike swarms, the 824 Ma Quruqtagh dolerite dikes, the 825 Ma Gaojiacun mafic–ultramafic intrusions and the 821 Ma Bikou continental flood basalts, and so on. All these rocks are products of the 850–820 Ma superplume, which marks the beginning of protracted fragmentation process.

(b) The precursory uplift and doming induced by upwelling of a hot and buoyant plume head were followed by the subsidence and extension of thinned continental lithosphere (Fig. 14b), which led to the unconformable contact of sequences and formed rift basins, and further rifted passive continental margins with seaward-dipping reflector sequences (Fig. 14c). The former is ascribed to the continent-scale unroofing and rapid erosion (Li et al., 1999). The latter process was characterized by major rift phase that peaked starting at ca. 820 Ma and included the later prolonged, multi-staged (820–800 Ma, 790–760 Ma and perhaps ca. 600 Ma) volcanism in the Australia, South

China, Qilian–Qaidam and Tarim cratons (Li et al., 2008b and references therein; Xu et al., 2015). These syn-rift magmatic activities were accompanied by the formation of volcanic-sedimentary successions in coeval rift basins (e.g., the Kangdian and Nanhua rifts in South China and the Adelaide geosyncline in Australia). As a result, microcontinents such as South China and Qilian–Qaidam were episodically split from the Australian mainland and the coeval LIP (850–820 Ma) records were dismembered (Fig. 14c).

(c) The subduction of oceanic lithosphere and the existence of passive continental margin were regarded as the prerequisites for continental deep subduction (Song et al., 2014). The ophiolitic sequences in the eastern segment of the North Qaidam UHPM belt may represent the Early Paleozoic oceanic crust (Zhang et al., 2008). Except for the Yingfeng dolerites/basalts, the drag or rollback of oceanic slabs caused the Neoproterozoic continental flood basalts and subordinate dikes, together with Grenville-age granites and sedimentary rocks, to experience medium to ultra-high pressure metamorphism during the continental collision/subduction, starting at ~440 Ma (Fig. 14d and e).

8. Conclusion

(1) The occurrence, geochronological and geochemical data reveal that the Yingfeng dikes/basalts and Aolaoshan metavolcanics, together with the eclogite blocks in the UHPM belt, constitute a possible Neoproterozoic LIP, namely the North Qaidam LIP.

(2) The North Qaidam LIP lends support for the large scale onset of mantle plume within the Rodinia supercontinent at ~850 Ma. It also represents one of the fragments dismembered by the breakup of the Rodinia on the volcanic-rifted passive margin.

(3) The igneous rocks of the North Qaidam LIP on the north margin of the Qaidam block experienced the greenschist-, amphibolite-, HP granulite- to UHP eclogite-facies metamorphism along the subducted continental margin from the surface to depths greater than 120 km at 440–420 Ma.

(4) The North Qaidam LIP supports the idea that the Australia, South China, Tarim and Qilian–Qaidam blocks have close affinities in the Neoproterozoic.

Acknowledgements

We are grateful to X.H. Li and his laboratory group for helping with the zircon dating. This study was supported by the Major State Basic Research Development Program (2015CB856105), Basic geological survey program of China Geological Survey (1212011121258) and National Natural Science Foundation of China (Grant Nos. 41372060, 41572040, 41130314).

Appendix A. Supplementary data

Supplementary data associated with this article can be found, in the online version, at http://dx.doi.org/10.1016/j.precamres.2016.07.007.

References

Andersen, T., 2002. Correction of common lead in U-Pb analyses that do not report 204Pb. Chem. Geol. 192, 59–79.
Black, L.P., Kamo, S.L., Allen, C.M., Aleinikoff, J.N., Davis, D.W., Korsch, R.J., Foudoulis, C., 2003. TEMORA 1: a new zircon standard for Phanerozoic U-Pb geochronology. Chem. Geol. 200, 155–170.
Brown, M., 2009. Metamorphic patterns in orogenic systems and the geological record. Geol. Soc. London Spec. Publ. 318 (1), 37–74.
Bryan, S.E., Ernst, R.E., 2008. Revised definition of large igneous provinces (LIPs). Earth-Sci. Rev. 86 (1), 175–202.
Bryan, S.E., Ferrari, L., 2013. Large igneous provinces and silicic large igneous provinces: progress in our understanding over the last 25 years. Geol. Soc. Am. Bull. 125 (7–8), 1053–1078.
Cabanis, B., Lecolle, M., 1989. Le diagramme La/10–Y/15–Nb/8: un outil pour la discrimination des series volcaniques et la mise en evidence des procesus de mélange et/ou de contamination crutale. C. R. Acad. Sci. 309, 2023–2029.
Coffin, M.F., Eldholm, O., 1994. Large igneous provinces: crustal structure, dimensions, and external consequences. Rev. Geophys. 32, 1–36.
Courtillot, V., Jaupart, C., Manighetti, I., Tapponnier, P., Besse, J., 1999. On causal links between flood basalts and continental breakup. Earth Planet. Sci. Lett. 166, 177–195.
Chen, N.S., Wang, Q.Y., Chen, Q., Li, X.Y., 2007. Components and metamorphism of the basements of the Qaidam and Oulongbuluke micro-continental blocks, and a tentative interpretation of paleocontinental evolution in NW-Central China. Earth Sci. Front. 14, 43–55 (in Chinese with English abstract).
Chen, N.S., Gong, S.L., Sun, M., Li, X.Y., Xia, X.P., Wang, Q.Y., Wu, F.Y., Xu, P., 2009a. Precambrian evolution of the Quanji Block, northeastern margin of Tibet: insights from zircon U-Pb and Lu–Hf isotope compositions. J. Asian Earth Sci. 35 (3), 367–376.
Chen, D.L., Liu, L., Sun, Y., Liou, J.G., 2009b. Geochemistry and zircon U-Pb dating and its implications of the Yukahe HP/UHP terrane, the North Qaidam, NW China. J. Asian Earth Sci. 35, 259–272.
Dale, J., Holland, T., Powell, R., 2000. Hornblende-garnet-plagioclase thermobarometry: a natural assemblage calibration of the thermodynamics of hornblende. Contrib. Mineral. Petrol. 140, 353–362.
Eckert Jr., J.O., Newton, R.C., Kleppa, O.J., 1991. The H of reaction and recalibration of garnet-pyroxene-plagioclase-quartz geobarometers in the CMAS system by solution calorimetry. Am. Mineral. 76, 148–160.
Ernst, R.E., Buchan, K.L., Campbell, I.H., 2005. Frontiers in large igneous province research. Lithos 79, 271–297.
Ernst, R.E., Wingate, M.T.D., Buchan, K.L., Li, Z.X., 2008. Global record of 1600–700 Ma Large Igneous Provinces (LIPs): implications for the reconstruction of the proposed Nuna (Columbia) and Rodinia supercontinents. Precambr. Res. 160 (1), 159–178.
Ernst, R.E., Jowitt, S.M., 2013. Large Igneous Provinces (LIPs) and metallogeny. Soc. Econ. Geol. Spec. Publ. 17, 17–51.
Ernst, R.E., 2014. Large igneous provinces. Cambridge University Press.
Garfunkel, Z., 2008. Formation of continental flood volcanism—the perspective of setting of melting. Lithos 100 (1), 49–65.
George, R.M., Rogers, N.W., 2002. Plume dynamics beneath the African plate inferred from the geochemistry of the Tertiary basalts of southern Ethiopia. Contrib. Mineral. Petrol. 144, 286–304.
Hawkesworth, C.J., Lightfoot, P.C., Fedorenko, V.A., Blake, S., Naldrett, A.J., Doherty, W., Gorbachev, N.S., 1995. Magma differentiation and mineralisation in the Siberian continental flood basalts. Lithos 34, 61–88.
Herzberg, C., O'Hara, M.J., 2002. Plume-associated ultramafic magmas of Phanerozoic age. J. Petrol. 43, 1857–1883.
Herzberg, C., Asimow, P.D., Arndt, N., Niu, Y., Lesher, C.M., Fitton, J.G., Saunders, A.D., 2007. Temperature in ambient mantle and plumes: constraints from basalts, picrites, and komatiites. Geochem. Geophys. Geosyst. 8 (2), 1074–1086.
Hofmann, A.W., 1988. Chemical differentiation of the Earth: the relationship between mantle, continental crust, and oceanic crust. Earth Planet. Sci. Lett. 90, 297–314.
Holland, T.J.B., Blundy, J.D., 1994. Non-ideal interactions in calcic amphiboles and their bearing on amphibole-plagioclase thermometry. Contrib. Mineral. Petrol. 116, 433–447.
Hill, R.I., Campbell, I.H., Davies, G.F., Griffiths, R.W., 1992. Mantle plumes and continental tectonics. Science 256 (5054), 186–193.
Hu, N.G., Wang, X.X., Sun, Y.G., 2007. The geochemistry features, origin of the Yingfeng rapakivi granite and its associated rocks in north Qaidam basin and the geological significance. Geol. Rev. 53 (4), 731–745.
Ingle, S., Weis, D., Scoates, J.S., Frey, F.A., 2002. Relationship between the early Kerguelen plume and continental flood basalts of the paleo-eastern Gondwanan margins. Earth Planet. Sci. Lett. 197, 35–50.
Jowitt, S.M., Ernst, R.E., 2013. Geochemical assessment of the metallogenic potential of Proterozoic LIPs of Canada. Lithos 174 (4), 291–307.
Le Bas, M.J., 2000. IUGS reclassification of the high-Mg and picritic volcanic rocks. J. Petrol. 41 (10), 1467–1470.
Leech, M.L., Singh, S., Jain, A.K., Klemperer, S.L., Manickavasagam, R.M., 2005. The onset of India-Asia continental collision: early, steep subduction required by the timing of UHP metamorphism in the western Himalaya. Earth Planet. Sci. Lett. 234, 83–97.
Li, H.K., Lu, S.N., Wang, H.C., Xiang, Z.Q., Zheng, J.K., 2003a. Quanji Group—the geological record of the Rodinia Supercontinent breakup in the early Neoproterozoic preserved in the north Qaidam margin, Qinghai, Northwest China. Geol. Surv. Res. 26, 27–37 (in Chinese).
Li, Q.L., Li, X.H., Liu, Y., Tang, G.Q., Yang, J.H., Zhu, W.G., 2010a. Precise U-Pb and Pb-Pb dating of Phanerozoic baddeleyite by SIMS with oxygen flooding technique. J. Anal. At. Spectrom. 25, 1107–1113.
Li, W.X., Li, X.H., Li, Z.X., 2010b. Ca. 850 Ma bimodal volcanic rocks in northeastern Jiangxi Province, South China: initial extension during the breakup of Rodinia. Am. J. Sci. 310, 951–980.

Li, X.H., Li, W.X., Li, Q.L., Wang, X.C., Liu, Y., Yang, Y.H., 2010c. Petrogenesis and tectonic significance of the ~850 Ma Gangbian alkaline complex in South China: evidence from in situ zircon U-Pb dating, Hf–O isotopes and whole-rock geochemistry. Lithos 114, 1–15.
Li, X.H., Li, W.X., Li, Z.X., Liu, Y., 2008a. 850–790 Ma bimodal volcanic and intrusive rocks in northern Zhejiang, South China: a major episode of continental rift magmatism during the breakup of Rodinia. Lithos 102 (1), 341–357.
Li, X.H., Li, Z.X., Zhou, H., Liu, Y., Kinny, P.D., 2002. U-Pb zircon geochronology, geochemistry and Nd isotopic study of Neoproterozoic bimodal volcanic rocks in the Kangdian Rift of South China; implications for the initial rifting of Rodinia. Precambr. Res. 113, 135–154.
Li, X.H., Liu, Y., Li, Q.L., Guo, C.H., Chamberlain, K.R., 2009. Precise determination of Phanerozoic zircon Pb/Pb age by multicollector SIMS without external standardization. Geochem. Geophys. Geosyst. 10 (4).
Li, X.H., Su, L., Chung, S.L., Li, Z.X., Liu, Y., Song, B., Liu, D.Y., 2005. Formation of the Jinchuan ultramafic intrusion and the world's third largest Ni-Cu sulfide deposit: Associated with the~ 825 Ma south China mantle plume? Geochem. Geophys. Geosyst. 6 (11).
Li, X.H., Tang, G.Q., Gong, B., Yang, Y.H., Hou, K.J., Hu, Z.C., Li, Q.L., Liu, Y., Li, W.X., 2013. Qinghu zircon: a working reference for microbeam analysis of U-Pb age and Hf and O isotopes. Chin. Sci. Bull. 58, 4647–4654.
Li, Z.X., Bogdanova, S.V., Collins, A.S., Davidson, A., De Waele, B., Ernst, R.E., Fitzsimons, I.C.W., Fuck, R.A., Gladkochub, D.P., Jacobs, J., Karlstrom, K.E., Lu, S., Natapov, L.M., Pease, V., Pisarevsky, S.A., Thrane, K., Vernikovsky, V., 2008b. Assembly, configuration, and break-up history of Rodinia: a synthesis. Precambr. Res. 160, 179–210.
Li, Z.X., Li, X.H., Kinny, P.D., Wang, J., 1999. The breakup of Rodinia: did it start with a mantle plume beneath South China? Earth Planet. Sci. Lett. 173, 171–181.
Li, Z.X., Li, X.H., Kinny, P.D., Wang, J., Zhang, S., Zhou, H., 2003b. Geochronology of Neoproterozoic syn-rift magmatism in the Yangtze Craton South China and correlations with other continents: evidence for a mantle superplume that broke up Rodinia. Precambr. Res. 122, 85–109.
Lu, S.N., Li, H.K., Zhang, C.L., Niu, G.H., 2008. Geological and geochronological evidence for the Precambrian evolution of the Tarim Craton and surrounding continental fragments. Precambr. Res. 160, 94–107.
Ludwig, K.R., 2001. User's Manual for Isoplot/Ex rev. 2.49. Berkeley Geochronology Centre, pp. 56, Special Publication 1.
Melluso, L., Mahoney, J.J., Dallai, L., 2006. Mantle sources and crustal input as recorded in high-Mg Deccan Traps basalts of Gujarat (India). Lithos 89, 259–274.
Miyashiro, A., 1974. Volcanic rock series in island arcs and active continental margins. Am. J. Sci. 274 (4), 321–355.
Nesbitt, H.W., Young, G.M., 1982. Early Proterozoic climates and plate motions inferred from major element chemistry of lutites. Nature 299 (5885), 715–717.
Nesbitt, H.W., Young, G.M., 1989. Formation and diagenesis of weathering profiles. J. Geol., 129–147
Niu, Y.L., O'Hara, M.J., 2008. Global correlations of ocean ridge basalt chemistry with axial depth: a new perspective. J. Petrol. 49, 633–664.
Park, J.K., Buchan, K.L., Harlan, S.S., 1995. A proposed giant radiating dyke swarm fragmented by the separation of Laurentia and Australia based on paleomagnetism of ca 780 Ma mafic intrusions in western North America. Earth Planet. Sci. Lett. 132 (1), 129–139.
Pearce, J.A., 2008. Geochemical fingerprinting of oceanic basalts with applications to ophiolite classification and the search for Archean oceanic crust. Lithos 100, 14–48.
Peng, P., Bleeker, W., Ernst, R.E., Soderlund, U., McNicoll, V., 2011. U-Pb baddeleyite ages, distribution and geochemistry of 925 Ma mafic dykes and 900 Ma sills in the North China craton: Evidence for a Neoproterozoic mantle plume. Lithos 127, 210–221.
Powell, C.M., Preiss, W.V., Gatehouse, C.G., Krapez, B., Li, Z.X., 1994. South Australian record of a Rodinian epicontinental basin and its mid-Neoproterozoic breakup (~700 Ma) to form the Palaeo-Pacific Ocean. Tectonophysics 237, 113–140.
Preiss, W.V., 2000. The Adelaide Geosyncline of South Australia and its significance in Neoproterozoic continental reconstruction. Precambr. Res. 100, 21–63.
Ravna, E.K., 2000. The garnet-clinopyroxene Fe^{2+}–Mg geothermometer: an updated calibration. J. Metamorph. Geol. 18, 211–219.
Richards, M.A., Duncan, R.A., Courtillot, V.E., 1989. Flood basalts and hot-spot tracks; plume heads and tails. Science 246, 103–107.
Rudnick, R.L., Gao, S., 2003. Composition of the continental crust. Treatise Geochem. 3 (1), 1–23.
Saunders, A.D., Tarney, J., Kerr, A.C., Kent, R.W., 1996. The formation and fate of large oceanic igneous provinces. Lithos 37 (2), 81–95.
Saunders, A.D., 2005. Large igneous provinces: origin and environmental consequences. Elements 1, 259–263.
Shu, L.S., Faure, M., Yu, J.H., Jahn, B.M., 2011. Geochronological and geochemical features of the Cathaysia block (South China): new evidence for the Neoproterozoic breakup of Rodinia. Precambr. Res. 187, 263–276.
Sharma, M., Basu, A.R., Nesterenko, G.V., 1992. Temporal Sr-, Nd- and Pb-isotopic variations in the Siberian flood basalts: implications for the plume-source characteristics. Earth Planet. Sci. Lett. 113, 365–381.
Shervais, J.W., 1982. Ti–V plots and the petrogenesis of modern and ophiolitic lavas. Earth Planet. Sci. Lett. 59, 101–118.
Sláma, J., Košler, J., Condon, D.J., Crowley, J.L., Gerdes, A., Hanchar, J.M., Horstwood, M.S.A., Morris, G.A., Nasdala, L., Norberg, N., Schaltegger, U., Schoene, B., Tubrett, M.N., Whitehouse, M.J., 2008. Plešovice zircon – A new natural reference material for U-Pb and Hf isotopic microanalysis. Chem. Geol. 249, 1–35.
Stacey, J.S., Kramers, J.D., 1975. Approximation of terrestrial lead isotope evolution by a two-stage model. Earth Planet. Sci. Lett. 26, 207–221.
Song, S.G., Zhang, L.F., Niu, Y.L., Su, L., Song, B., Liu, D.Y., 2006. Evolution from oceanic subduction to continental collision: a case study of the Northern Tibetan Plateau inferred from geochemical and geochronological data. J. Petrol. 47, 435–455.
Song, S.G., Zhang, G.B., Su, L., Niu, Y.L., Zhang, L.F., 2009. Two types of peridotite in North Qaidam UHPM belt and their tectonic implications for oceanic and continental subduction: a review. J. Asian Earth Sci. 35, 285–297.
Song, S.G., Su, L., Li, X.H., Zhang, G.B., Niu, Y.L., Zhang, L.F., 2010. Tracing the 850-Ma continental flood basalts from a piece of subducted continental crust in the North Qaidam UHPM belt, NW China. Precambr. Res. 183, 805–816.
Song, S.G., Su, L., Li, X.H., Niu, Y.L., Zhang, L.F., 2012. Grenville-age orogenesis in the Qaidam–Qilian block: the link between South China and Tarim. Precambr. Res. 220, 9–22.
Song, S.G., Niu, Y.L., Su, L., Xia, X.H., 2013. Tectonics of the North Qilian orogen, NW China. Gondwana Res. 23, 1378–1401.
Song, S.G., Niu, Y.L., Su, L., Zhang, C., Zhang, L.F., 2014. Continental orogenesis from ocean subduction, continent collision/subduction, to orogen collapse, and orogen recycling: the example of the North Qaidam UHPM belt, NW China. Earth Sci. Rev. 129, 59–84.
Sun, S.S., McDonough, W.F., 1989. Chemical and Isotopic Systematics of Oceanic Basalts: Implications for Mantle Composition and Processes. Geological Society, London, pp. 313–345, Special Publications 42.
Sylvester, P.J., 1998. Post-collisional strongly peraluminous granites. Lithos 45, 29–44.
Tung, K.A., Yang, H.Y., Liu, D.Y., Zhang, J.X., Yang, H.J., Shau, Y.H., Tseng, C.Y., 2013. The Neoproterozoic granitoids from the Qilian block, NW China: evidence for a link between the Qilian and South China blocks. Precambr. Res. 235, 163–189.
Wang, X.C., Li, X.H., Li, W.X., Li, Z.X., Liu, Y., Yang, Y.H., Liang, X.R., Tu, X.L., 2008. The Bikou basalts in the northwestern Yangtze block, South China: remnants of 820–810 Ma continental flood basalts? Geol. Soc. Am. Bull. 120, 1478–1492.
Wang, X.C., Li, X.H., Li, W.X., Li, Z.X., 2009. Variable involvements of mantle plumes in the genesis of mid-Neoproterozoic basaltic rocks in South China: a review. Gondwana Res. 15, 381–394.
Wang, X.L., Zhou, J.C., Griffin, W.L., Wang, R.C., Qiu, J.S., O'Reilly, S.Y., Xu, X.S., Liu, X. M., Zhang, G.L., 2007. Detrital zircon geochronology of Precambrian basement sequences in the Jiangnan orogen: dating the assembly of the Yangtze and Cathaysia Blocks. Precambr. Res. 159 (1), 117–131.
Wang, J., Li, Z.X., 2003. History of Neoproterozoic rift basins in South China: implications for Rodinia break-up. Precambr. Res. 122, 141–158.
Wan, Y.S., Xu, Z.Q., Yang, J.S., Zhang, J.X., 2001. Ages and compositions of the Precambrian high-grade basement of the Qilian terrane and its adjacent areas. Acta Geol. Sinica 75, 375–384.
Wan, Y.S., Zhang, J.X., Yang, J.S., Xu, Z.Q., 2006. Geochemistry of high-grade metamorphic rocks of the North Qaidam Mountains and their geological significance. J. Asian Earth Sci. 28, 174–184.
Weis, D., Kieffer, B., Maerschalk, C., Barling, J., Jong, J.D., Williams, G.A., Hanano, D., Pretorius, W., Mattielli, N., Scoates, J.S., Goolaerts, A., Friedman, R.M., Mahoney, J.B., 2006. High-precision isotopic characterization of USGS reference materials by TIMS and MC-ICP-MS. Geochem. Geophys. Geosyst. 7 (8), 139–149.
Wood, D.A., 1980. The application of a Th-Hf-Ta diagram to problems of tectonomagmatic classification and to establishing the nature of crustal contamination of basaltic lavas of the British Tertiary Volcanic Province. Earth Planet. Sci. Lett. 50 (1), 11–30.
Wiedenbeck, M., Alle, P., Corfu, F., Griffin, W.L., Meier, M., Oberli, F., Vonquadt, A., Roddick, J.C., Speigel, W., 1995. Three natural zircon standards for U-Th-Pb, Lu-Hf, trace-element and REE analyses. Geostand. Newslett. 19 (1), 1–23.
Wingate, M.T.D., Campbell, I.H., Compston, W., Gibson, G.M., 1998. Ion microprobe U-Pb ages for Neoproterozoic basaltic magmatism in southcentral Australia and implications for the breakup of Rodinia. Precambr. Res. 87, 135–159.
Winchester, J.A., Floyd, P.A., 1976. Geochemical magma type discrimination: application to altered and metamorphosed basic igneous rocks. Earth Planet. Sci. Lett. 28, 459–469.
Wilson, M., 1989. Igneous Petrogenesis. Unwin Hyman, London.
White, R.S., McKenzie, D.P., 1989. Magmatism at rift zones: the generation of volcanic continental margins and flood basalts. J. Geophys. Res. 94, 7685–7729.
Xiao, Q.H., Lu, X.X., Wang, F., 2003. Age of Yinfeng Rapakivi Granite and its significance in the north margin of Qaidam. Sci. China (Ser. D), 22–28 (in Chinese).
Xu, Y.G., Chung, S.L., Jahn, B.M., Wu, G.Y., 2001. Petrologic and geochemical constraints on the petrogenesis of Permian-Triassic Emeishan flood basalts in southwestern China. Lithos 58, 145–168.
Xu, X., Song, S.G., Su, L., Li, Z.X., Niu, Y.L., Allen, M.B., 2015. The 600–580 Ma continental rift basalts in North Qilian Shan, northwest China: Links between the Qilian-Qaidam block and SE Australia, and the reconstruction of East Gondwana. Precambr. Res. 257, 47–64.
Yu, S.Y., Zhang, J.X., Li, H.K., Hou, K.J., Mattinson, C.G., Gong, J.H., 2013. Geochemistry, zircon U-Pb geochronology and Lu-Hf isotopic composition of eclogites and their host gneisses in the Dulan area, North Qaidam UHP terrane: New evidence for deep continental subduction. Gondwana Res. 23 (3), 901–919.
Zhang, J.X., Zhang, Z.M., Xu, Z.Q., Yang, J.S., Cui, J.W., 2001. Petrology and geochronology of eclogites from the western segment of the Altyn Tagh, Northwestern China. Lithos 56, 187–206.
Zhang, J.X., Mattinson, C.G., Yu, S.Y., Li, J.P., Meng, F.C., 2010. U-Pb zircon geochronology of coesite-bearing eclogites from the southern Dulan area of

the North Qaidam UHP terrane, northwestern China: spatially and temporally extensive UHP metamorphism during continental subduction. J. Metamorph. Geol. 28 (9), 955–978.

Zhang, G.B., Song, S.G., Zhang, L.F., Niu, Y.L., 2008. The subducted oceanic crust within continental-type UHP metamorphic belt in the North Qaidam NW China: evidence from petrology, geochemistry and geochronology. Lithos 104, 99–108.

Zhang, C., Zhang, L.F., Roermund, H., Song, S.G., Zhang, G.B., 2011. Petrology and SHRIMP U-Pb dating of the eclogite in the Xitieshan area of the North Qaidam HP–UHP metamorphic belt, Western China. J. Asian Earth Sci. 42, 752–767.

Zhang, C., Zhang, L.F., Bader, T., Song, S.G., Lou, Y.X., 2012. Geochemistry and trace element behaviors of eclogite during its exhumation in the Xitieshan terrane, North Qaidam UHP belt, NW China. J. Asian Earth Sci. 63, 81–97.

Zhang, C., Bader, T., Zhang, L.F., van Roermund, H., 2015. The multi-stage tectonic evolution of the Xitieshan terrane, North Qaidam orogen, western China: From Grenville-age orogeny to early-Paleozoic ultrahigh-pressure metamorphism. Gondwana Res. http://dx.doi.org/10.1016/j.gr.2015.04.011.

Zhang, Z.Y., Zhu, W.B., Shu, L.S., Su, J.B., Zheng, B.H., 2009. Neoproterozoic ages of the Kuluketage diabase dyke swarm in Tarim, NW China, and its relationship to the breakup of Rodinia. Geol. Mag. 146 (01), 150–154.

Zhu, W.G., Zhong, H., Deng, H.L., Wilson, A.H., Liu, B.G., Li, C.Y., Qin, Y., 2006. SHRIMP zircon U-Pb age, geochemistry, and Nd-Sr isotopes of the Gaojiacun mafic-ultramafic intrusive complex, Southwest China. Int. Geol. Rev. 48 (7), 650–668.

Zhou, M.F., Yan, D.P., Kennedy, A.K., Li, Y., Ding, J., 2002. SHRIMPU–Pb zircon geochronological and geochemical evidence for Neoproterozoic arc magmatism along the western margin of the Yangtze Block, South China. Earth Planet. Sci. Lett. 196, 51–67.

Zhou, M.F., Ma, Y., Yan, D.P., Xia, X., Zhao, J.H., Sun, M., 2006a. The Yanbian Terrane (Southern Sichuan Province, SW China): A Neoproterozoic arc assemblage in the western margin of the Yangtze Block. Precambr. Res. 144, 19–38.

Zhou, M.F., Yan, D.P., Wang, C.L., Xia, X., Zhao, J.H., Sun, M., 2006b. Subduction-related origin of the 750 Ma Xuelongbao adakitic complex (Sichuan Province, China): implications for the tectonic setting of the giant Neoproterozoic magmatic event in South China. Earth Planet. Sci. Lett. 248, 271–285.